specific fluorescence signal of MRP2 was observed in the EHBR liver after infection of only Ad-tTA (Fig. 2).

Transport Activity Associated with the Isolated CMVs

After confirming the protein expression level of MRP2, the uptake of MRP2 substrates was examined using thr isolated CMVs. Typical substrates of MRP2, [^{3}H]$E_2$17ßG and [^{3}H]DNP-SG, were clearly taken up into CMVs prepared from MRP2-EHBR in an ATP-dependent manner (Fig. 3). In particular, the ATP-dependent uptake of CMVs was higher when infected with 7.5×10^9 pfu than with 1.0×10^9 pfu, which is consistent with the result of the Western blot analysis (Fig. 1). Moreover, the extent of the uptake of [^{3}H]$E_2$17ßG and [^{3}H]DNP-SG was almost identical to that of the CMVs prepared from normal SD rats when infected with 7.5×10^9 pfu of Ad-MRP2 (Fig. 3).

Biliary Excretion of DBSP

The plasma disappearance of DBSP was compared between control-EHBR and MRP2-EHBR. Figure 4A shows that the plasma disappearance curves for DBSP after *i.v.* administration were similar for control-EHBR and MRP2-EHBR up to 21 min. In contrast, the maximum biliary excretion rate in MRP2-EHBR was approximately 3-fold higher than that in control-EHBR (Fig. 4B). The cumulative amount of DBSP excreted into the bile up to 2 h in MRP2-EHBR was greater than that in control-EHBR (Fig. 4C). The biliary excretion clearance value, defined by dividing the total amount excreted into bile by AUC of DBSP, in MRP2-EHBR increased 3-fold compared with that in control-EHBR (Table I).

Bilirubin Concentration in Serum and Bile

The concentration of both direct and indirect bilirubin in the serum of normal rats, EHBR, control-EHBR, and MRP2-EHBR was also measured. The concentration of both direct and indirect bilirubin in the serum was significantly lower in MRP2-EHBR compared with control-EHBR (7.1 mg/ml vs. 97.4 mg/ml) (Table I). The decrease in direct bilirubin after

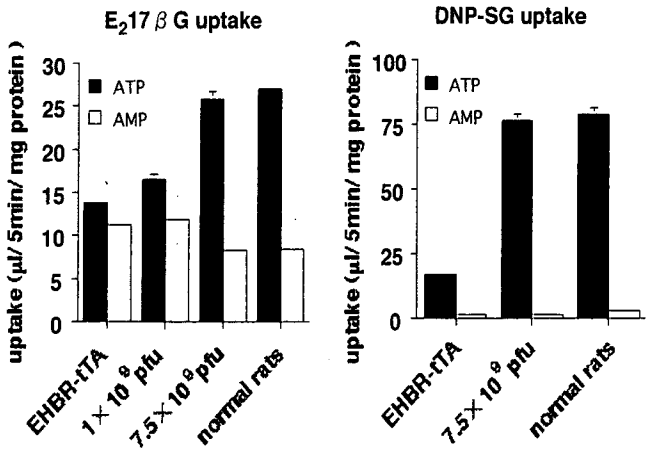

Fig. 3. Transport activity of human MRP2 in CMVs. [^{3}H]$E_2$17ßG and [^{3}H]DNP-SG uptake was measured in CMVs from MRP2-EHBR and control-EHBR. CMVs were incubated at 37°C with [^{3}H]$E_2$17ßG (400 nM) and [^{3}H]DNP-SG (500 nM) in the medium containing ATP (solid bar) and AMP (open bar) for 5 min. The results are shown as the mean ± SE of triplicate determinations.

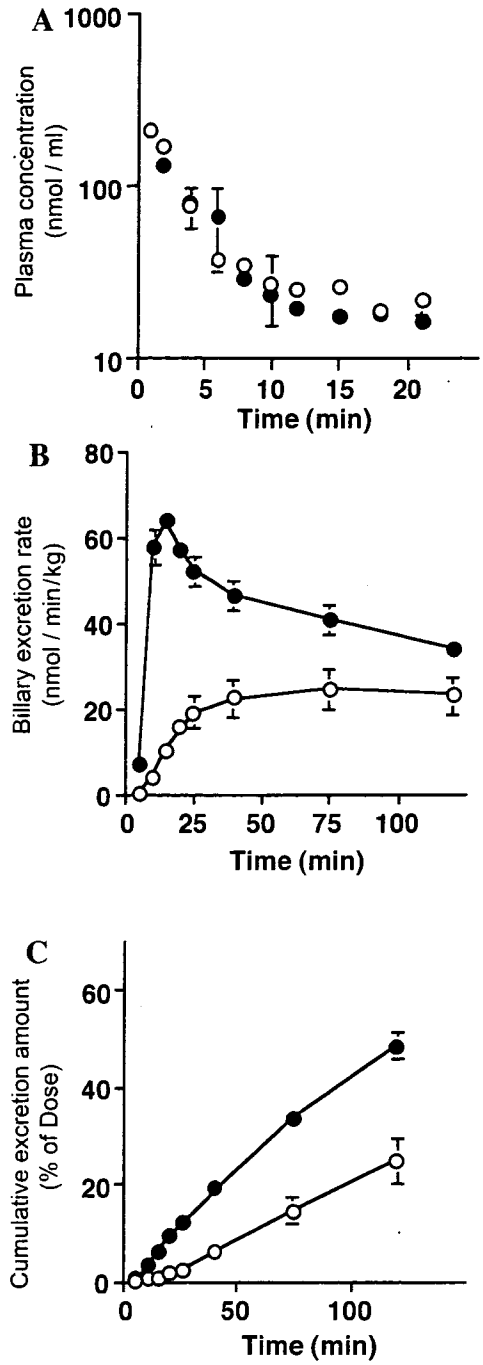

Fig. 4. Biliary excretion of DBSP. DBSP (10 µmol/kg) was administered intravenously as a bolus to MRP2-EHBR (●) and control-EHBR (○). (A) shows the plasma disappearance curves for DBSP. (B) and (C) show the time-course for the biliary excretion rate and that for cumulative biliary excretion, respectively. Each point and bar represents the mean ± SE of 3 rats.

human MRP2 expression was much greater than that in indirect bilirubin (from 97.4 mg/ml to 7.1 mg/ml, vs. 10.8 mg/ml to 4.9 mg/ml) (Table I), presumably because the direct bilirubin can be excreted into bile via human MRP2 (23). However, the concentration of direct bilirubin in control-EHBR plasma was much greater than that in untreated EHBR (97.4 mg/ml vs. 30.1 mg/ml) (Table I). In our preliminary results, infection of adenoviruses induced the expression of Mrp3, which is ex-

Table I. Bile Flow Rate, Concentration of Bilirubin in Serum, and the Biliary Excretion Clearance of DBSP

	SD rat	MRP2-EHBR	Control-EHBR	EHBR
Bile flow rate ($\mu l\ min^{-1}\ g\ liver^{-1}$)	1.14 ± 0.10	1.08 ± 0.13	0.79 ± 0.10	0.79 ± 0.08
Serum bilirubin (μM)				
Direct	1.0 ± 0.5	7.1 ± 0.9**	97.4 ± 8.2	30.1 ± 4.5
Indirect	1.1 ± 0.5	4.9 ± 2.3	10.8 ± 1.7	6.2 ± 3.2
CL_H ($ml\ min^{-1}\ kg^{-1}$)	32.1 ± 7.8	3.2 ± 0.5*	1.1 ± 0.2	2.4 ± 0.2

The biliary excretion clearance of DBSP are analyzed from the data of Fig. 4.
* $p < 0.05$ vs. control-EHBR; **$p < 0.01$ vs. control-EHBR by student's t-test.

pressed at the sinusoidal membrane of the liver. Since direct bilirubin can be excreted into blood via Mrp3 (24), the increase in the plasma direct bilirubin levels in control-EHBR may be accounted for by the increase of sinusoidal Mrp3 expression induced by adenovirus infection.

DISCUSSION

The function of Mrp2/MRP2 has been studied extensively by comparing the transport across the bile canalicular membrane between normal and Mrp2-deficient rats (such as Groningen Yellow (GY), transport deficient (TR-), and Eisai hyperbilirubinemic rats (EHBRs)) (16,17,25,26). Furthermore, MRP2 function has been characterized by using the cDNA-transfected cells (1,3,6,22). The canalicular localization of MRP2 (23) has been reflected by the apical localization in polarized mammalian cell lines (22). It is also reported that the pathogenesis of some DJS is accounted for by the lack in the normal apical sorting of MRP2 molecules (10,11). The localization of MRP2 have been characterized by the polarized mammalian cell lines (22), and by the liver sample from DJS patients (10,11). Moreover, we have analyzed the function of MRP2 SNPs variants/mutants using the LLC-PK1 cell line, and found that some variants were localized not only at the apical membrane but also in the intracellular compartment of this polarized cell line (12). Since the SNPs/mutations of MRP2 may have an effect on drug disposition, identification of the *in vivo* localization of MRP2 variants is quite important. In the current study, we have constructed a model for evaluating the function of human MRP2 using EHBR.

We first investigated whether the localization of human MRP2 in liver is preserved in EHBR or not. The human MRP2 was expressed on the canalicular membrane after the adenovirus infection (Fig. 2), which is consistent with the physiologic localization of rat and human MRP2 (23), suggesting that the sorting mechanism of human MRP2 is also present in rat liver. Although we were unable to compare the absolute value of MRP2 protein expression between normal rats (rat MRP2) and MRP2-EHBR (human MRP2), the transport activity of CMVs from normal rats and MRP2-EHBR infected with 7.5×10^9 pfu was almost identical after the normalization of the membrane protein amount of CMVs (Fig. 3), suggesting that the expression level of human MPR2 may be enough for performing the *in vivo* experiments.

From the uptake study with CMVs, we are only able to estimate the drug transport from the liver across the bile canalicular membrane, whereas by performing the *in vivo* study, we are also able to evaluate the vectorical transport of drugs from blood to bile, which is essential for estimating the *in vivo* human biliary excretion. We have previously suggested that the biliary excretion of DBSP is reduced in EHBR compared with that in normal rats *in vivo* (27). Moreover, from the kinetic analysis, the reduction in the biliary excretion of organic anions may be due to a defect in the transport carriers on the bile canalicular membrane (27), suggesting that DBSP is predominantly excreted into bile via MRP2. Therefore, we selected DBSP as a model compound for examining its biliary excretion in a bolus infusion study. After iv injection of DBSP, the plasma concentration was similar between control-EHBR and MRP2-EHBR (Fig. 4A). Because the initial elimination of DBSP from plasma represents the hepatic uptake of this dye (27), this result suggests that the hepatic uptake activity is comparable between control-EHBR and MRP2-EHBR. However, a significant difference in the biliary excretion rate and that in the cumulative excretion were observed (Figs. 4B and 4C), suggesting that human MRP2 introduced by adenovirus recognizes DBSP as a substrate, and excretes DBSP from liver to bile via human MRP2. Moreover, the serum concentration of direct bilirubin was greatly reduced in MRP2-EHBR compared with that in control EHBR (Table I). This result suggests that human MRP2 excretes direct bilirubin into bile, resulting in an improvement of the symptoms of hyperbilirubinemia. However, the biliary excretion clearance in DBSP by MRP2-EHBR was only 3-fold of that of control-EHBR (Table I). It was in contrast to the fact that the biliary excretion clearance of DBSP was 10-fold higher in normal rats than that in EHBR, which is consistent with our previous result (27). Because the result of the *in vitro* transport activity for $E_2$17ßG and DNP-SG indicated that the expression level of human MRP2 is high enough (Fig. 3), we expected that the biliary excretion clearance of DBSP would be comparable between normal rats and MRP2-EHBR. This unexpected finding can be explained by considering the induction of sinusoidal Mrp3 by the adenovirus infection. It is possible that DBSP is excreted into blood via Mrp3, as a similar substrate specificity of Mrp2 and Mrp3 has been reported (28–30). The fact that the serum concentration of direct bilirubin was much greater in control-EHBR than that in untreated EHBR (97.4 mg/ml vs. 30.1 mg/ml) (Table I), may also be explained by Mrp3 induction by infection with the adenoviruses. Alternatively, the transport activity of DBSP by human MRP2 is lower than that by rat Mrp2, resulting the lower biliary excretion clearance of DBSP by MRP2-EHBR compared with normal rats.

In conclusion, we have been able to express human MRP2 at the canalicular membrane in EHBR liver. By comparing the expression level of MRP2 between MRP2-EHBR

and in human liver, this system may be useful in quantatively predicting the *in vivo* human biliary excretion of human MRP2 substrates. Moreover, because the wild-type human MRP2 was expressed at the canalicular membrane of EHBR liver, it may be possible to predict the localization and function of SNPs variants/mutants of human MRP2 in the intact liver.

REFERENCES

1. H. Suzuki and Y. Sugiyama. Transporters for bile acids and organic anions. *Pharm. Biotechnol.* **12**:387–439 (1999).
2. Y. Gotoh, H. Suzuki, S. Kinoshita, T. Hirohashi, Y. Kato, and Y. Sugiyama. Involvement of an organic anion transporter (canalicular multispecific organic anion transporter/multidrug resistance-associated protein 2) in gastrointestinal secretion of glutathione conjugates in rats. *J. Pharmacol. Exp. Ther.* **292**:433–439 (2000).
3. D. Keppler and J. Konig. Hepatic secretion of conjugated drugs and endogenous substances. *Semin. Liver Dis.* **20**:265–272 (2000).
4. H. Suzuki and Y. Sugiyama. Role of metabolic enzymes and efflux transporters in the absorption of drugs from the small intestine. *Eur. J. Pharm. Sci.* **12**:3–12 (2000).
5. C. G. Dietrich, D. R. de Waart, R. Ottenhoff, I. G. Schoots, and R. P. Elferink. Increased bioavailability of the food-derived carcinogen 2-amino-1-methyl-6-phenylimidazo[4,5-b]pyridine in MRP2-deficient rats. *Mol. Pharmacol.* **59**:974–980 (2001).
6. L. Payen, L. Sparfel, A. Courtois, L. Vernhet, A. Guillouzo, and O. Fardel. The drug efflux pump MRP2: regulation of expression in physiopathological situations and by endogenous and exogenous compounds. *Cell Biol. Toxicol.* **18**:221–233 (2002).
7. H. Suzuki and Y. Sugiyama. Single nucleotide polymorphisms in multidrug resistance associated protein 2 (MRP2/ABCC2): its impact on drug disposition. *Adv. Drug Deliv. Rev.* **54**:1311–1331 (2002).
8. P. Borst and R. O. Elferink. Mammalian ABC transporters in health and disease. *Annu. Rev. Biochem.* **71**:537–592 (2002).
9. R. O. Elferink and A. K. Groen. Genetic defects in hepatobiliary transport. *Biochim. Biophys. Acta* **1586**:129–145 (2002).
10. V. Keitel, J. Kartenbeck, A. T. Nies, H. Spring, M. Brom, and D. Keppler. Impaired protein maturation of the conjugate export pump multidrug resistance protein 2 as a consequence of a deletion mutation in Dubin-Johnson syndrome. *Hepatology* **32**:1317–1328 (2000).
11. K. Hashimoto, T. Uchiumi, T. Konno, T. Ebihara, T. Nakamura, M. Wada, S. Sakisaka, F. Maniwa, T. Amachi, K. Ueda, and M. Kuwano. Trafficking and functional defects by mutations of the ATP-binding domains in MRP2 in patients with Dubin-Johnson syndrome. *Hepatology* **36**:1236–1245 (2002).
12. M. Hirouchi, H. Suzuki, and Y. Sugiyama. Characterization of the cellular localization, expression level, and function of SNP variants of MRP2/ABCC2. *Pharm. Res.* **12**:387–439 (2004).
13. S. Masuda, K. Ibaramoto, A. Takeuchi, H. Saito, Y. Hashimoto, and K. I. Inui. Cloning and functional characterization of a new multispecific organic anion transporter, OAT-K2, in rat kidney. *Mol. Pharmacol.* **55**:743–752 (1999).
14. S. Masuda, H. Saito, and K. I. Inui. Interactions of nonsteroidal anti-inflammatory drugs with rat renal organic anion transporter, OAT-K1. *J. Pharmacol. Exp. Ther.* **283**:1039–1042 (1997).
15. H. H. Gu, J. Ahn, M. J. Caplan, R. D. Blakely, A. I. Levey, and G. Rudnick. Cell-specific sorting of biogenic amine transporters expressed in epithelial cells. *J. Biol. Chem.* **271**:18100–18106 (1996).
16. M. Buchler, J. Konig, M. Brom, J. Kartenbeck, H. Spring, T. Horie, and D. Keppler. cDNA cloning of the hepatocyte canalicular isoform of the multidrug resistance protein, cMrp, reveals a novel conjugate export pump deficient in hyperbilirubinemic mutant rats. *J. Biol. Chem.* **271**:15091–15098 (1996).
17. K. Ito, H. Suzuki, T. Hirohashi, K. Kume, T. Shimizu, and Y. Sugiyama. Molecular cloning of canalicular multispecific organic anion transporter defective in EHBR. *Am. J. Physiol.* **272**: G16–G22 (1997).
18. K. Kobayashi, Y. Sogame, H. Hara, and K. Hayashi. Mechanism of glutathione S-conjugate transport in canalicular and basolateral rat liver plasma membranes. *J. Biol. Chem.* **265**:7737–7741 (1990).
19. H. Mizuguchi and M. A. Kay. Efficient construction of a recombinant adenovirus vector by an improved in vitro ligation method. *Hum. Gene Ther.* **9**:2577–2583 (1998).
20. H. Mizuguchi and M. A. Kay. A simple method for constructing E1- and E1/E4-deleted recombinant adenoviral vectors. *Hum. Gene Ther.* **10**:2013–2017 (1999).
21. T. Hirohashi, H. Suzuki, X. Y. Chu, I. Tamai, A. Tsuji, and Y. Sugiyama. Function and expression of multidrug resistance-associated protein family in human colon adenocarcinoma cells (Caco-2). *J. Pharmacol. Exp. Ther.* **292**:265–270 (2000).
22. R. Evers, M. Kool, L. van Deemter, H. Janssen, J. Calafat, L. C. Oomen, C. C. Paulusma, R. P. Oude Elferink, F. Baas, A. H. Schinkel, and P. Borst. Drug export activity of the human canalicular multispecific organic anion transporter in polarized kidney MDCK cells expressing cMOAT (MRP2) cDNA. *J. Clin. Invest.* **101**:1310–1319 (1998).
23. D. Keppler, J. Konig, and M. Buchler. The canalicular multidrug resistance protein, cMRP/MRP2, a novel conjugate export pump expressed in the apical membrane of hepatocytes. *Adv. Enzyme Regul.* **37**:321–333 (1997).
24. T. Kamisako, Y. Kobayashi, K. Takeuchi, T. Ishihara, K. Higuchi, Y. Tanaka, E. C. Gabazza, and Y. Adachi. Recent advances in bilirubin metabolism research: the molecular mechanism of hepatocyte bilirubin transport and its clinical relevance. *J. Gastroenterol.* **35**:659–664 (2000).
25. R. Mayer, J. Kartenbeck, M. Buchler, G. Jedlitschky, I. Leier, and D. Keppler. Expression of the MRP gene-encoded conjugate export pump in liver and its selective absence from the canalicular membrane in transport-deficient mutant hepatocytes. *J. Cell Biol.* **131**:137–150 (1995).
26. C. C. Paulusma, P. J. Bosma, G. J. Zaman, C. T. Bakker, M. Otter, G. L. Scheffer, R. J. Scheper, P. Borst, and R. P. Oude Elferink. Congenital jaundice in rats with a mutation in a multidrug resistance-associated protein gene. *Science* **271**:1126–1128 (1996).
27. K. Sathirakul, H. Suzuki, K. Yasuda, M. Hanano, O. Tagaya, T. Horie, and Y. Sugiyama. Kinetic analysis of hepatobiliary transport of organic anions in Eisai hyperbilirubinemic mutant rats. *J. Pharmacol. Exp. Ther.* **265**:1301–1312 (1993).
28. H. Akita, H. Suzuki, T. Hirohashi, H. Takikawa, and Y. Sugiyama. Transport activity of human MRP3 expressed in Sf9 cells: comparative studies with rat MRP3. *Pharm. Res.* **19**:34–41 (2002).
29. T. Hirohashi, H. Suzuki, H. Takikawa, and Y. Sugiyama. ATP-dependent transport of bile salts by rat multidrug resistance-associated protein 3 (Mrp3). *J. Biol. Chem.* **275**:2905–2910 (2000).
30. J. Konig, A. T. Nies, Y. Cui, I. Leier, and D. Keppler. Conjugate export pumps of the multidrug resistance protein (MRP) family: localization, substrate specificity, and MRP2-mediated drug resistance. *Biochim. Biophys. Acta* **1461**:377–394 (1999).

0022-3565/05/3143-1059–1067$20.00
THE JOURNAL OF PHARMACOLOGY AND EXPERIMENTAL THERAPEUTICS
Vol. 314, No. 3
85589/3044446
JPET 314:1059–1067, 2005
Printed in U.S.A.

Identification of the Hepatic Efflux Transporters of Organic Anions Using Double-Transfected Madin-Darby Canine Kidney II Cells Expressing Human Organic Anion-Transporting Polypeptide 1B1 (OATP1B1)/Multidrug Resistance-Associated Protein 2, OATP1B1/Multidrug Resistance 1, and OATP1B1/Breast Cancer Resistance Protein

Soichiro Matsushima, Kazuya Maeda, Chihiro Kondo, Masaru Hirano, Makoto Sasaki, Hiroshi Suzuki, and Yuichi Sugiyama

Graduate School of Pharmaceutical Sciences, The University of Tokyo, Bunkyo-ku, Tokyo, Japan

Received February 28, 2005; accepted May 17, 2005

ABSTRACT

Until recently, it was generally believed that the transport of various organic anions across the bile canalicular membrane was mainly mediated by multidrug resistance-associated protein 2 (MRP2/ABCC2). However, a number of new reports have shown that some organic anions are also substrates of multidrug resistance 1 (MDR1/ABCB1) and/or breast cancer resistance protein (BCRP/ABCG2), implying MDR1 and BCRP could also be involved in the biliary excretion of organic anions in humans. In the present study, we constructed new double-transfected Madin-Darby canine kidney II (MDCKII) cells expressing organic anion-transporting polypeptide 1B1 (OATP1B1)/MDR1 and OATP1B1/BCRP, and we investigated the transcellular transport of four kinds of organic anions, estradiol-17β-D-glucuronide (EG), estrone-3-sulfate (ES), pravastatin (PRA), and cerivastatin (CER), to identify which efflux transporters mediate the biliary excretion of compounds using double-transfected cells. We observed the vectorial transport of EG and ES in all the double transfectants. MRP2 showed the highest efflux clearance of EG among these efflux transporters, whereas BCRP-mediated clearance of ES was the highest in these double transfectants. In addition, two kinds of 3-hydroxy-3-methylglutaryl-CoA reductase inhibitors, CER and PRA, were also substrates of all these efflux transporters. The rank order of the efflux clearance of PRA mediated by each transporter was the same as that of EG, whereas the contribution of MDR1 to the efflux of CER was relatively greater than for PRA. This experimental system is very useful for identifying which transporters are involved in the biliary excretion of organic anions that cannot easily penetrate the plasma membrane.

Biliary excretion is one of the major pathways for the elimination of unnecessary compounds from blood circulation. In the common process of hepatic clearance, compounds are taken up into liver, converted to more hydrophilic metabolites by metabolizing enzymes responsible for oxidation (e.g., cytochrome P450) and/or conjugation (e.g., UDP-glucuronosyl transferases and sulfotransferases), and subsequently excreted into bile. Several kinds of ATP-binding cassette (ABC) transporters on the bile canalicular membrane play an important role in this biliary excretion. It is generally accepted that multidrug resistance-associated protein 2 (MRP2/ABCC2) is responsible for the biliary excretion of a wide variety of organic anions including glutathione and glucuronide conjugates (Suzuki and Sugiyama, 1998; Konig et al., 1999). This has been proven by comparing the transport activity across the bile canalicular membrane between

This study was supported by Health and Labor Sciences Research grants from the Ministry of Health, Labor, and Welfare for the Research on Advanced Medical Technology and by Grant-in-Aid for Young Scientists B (15790087) from the Ministry of Education, Culture, Sports, Science, and Technology.
Article, publication date, and citation information can be found at http://jpet.aspetjournals.org.
doi:10.1124/jpet.105.085589.

ABBREVIATIONS: ABC, ATP-binding cassette; MRP, multidrug resistance-associated protein; EHBR, Eisai hyperbilirubinemic rats; MDR, multidrug resistance; EG, estradiol-17β-D-glucuronide; E3040, 6-hydroxy-5,7-dimethyl-2-methylamino-4-(3-pyridylmethyl) benzothiazole; BCRP, breast cancer resistance protein; MDCK, Madin-Darby canine kidney; OATP, organic anion-transporting polypeptide; PRA, pravastatin; HMG, 3-hydroxy-3-methylglutaryl; ES, estrone-3-sulfate; CER, cerivastatin; PBS, phosphate-buffered saline; TTBS, Tris-buffered saline with 0.05% Tween 20; PS, permeability surface product.

normal and Mrp2-deficient rats such as Eisai hyperbilirubinemic rats (EHBR) or TR$^-$ rats (Suzuki and Sugiyama, 1998; Konig et al., 1999).

Recently, it has been found that some organic anions can also be substrates of other ABC transporters. Multidrug resistance 1 (MDR1/ABCB1) preferentially accepts hydrophobic cationic or neutral compounds (Tanigawara, 2000; Varadi et al., 2002). However, Cvetkovic et al. (1999) reported that fexofenadine, an anionic nonsedating antihistamine, could be transported by human MDR1 (Cvetkovic et al., 1999). It has also been reported that estradiol-17β-D-glucuronide (EG) is a substrate of MDR1 as well as MRP2 in humans (Huang et al., 1998). Regarding the sulfated conjugates, we previously found that the biliary excretion clearance of the sulfates of 6-hydroxy-5,7-dimethyl-2-methylamino-4-(3-pyridylmethyl) benzothiazole (E3040) and liquiritigenin were excreted into bile in EHBR to the same extent as in Sprague-Dawley rats (Shimamura et al., 1994; Takenaka et al., 1995), suggesting that biliary excretion of sulfate conjugates is not mainly mediated by Mrp2 in rats. Suzuki et al. (2003) demonstrated that breast cancer resistance protein (BCRP/ABCG2) accepts various kinds of organic anions and preferentially transports sulfate conjugates (Suzuki et al., 2003). Taking into consideration the finding that MDR1 and BCRP are expressed in the canalicular membrane (Thiebaut et al., 1987; Maliepaard et al., 2001) in addition to these other facts, not only MRP2 but also MDR1 and BCRP can be involved in the biliary excretion of organic anions.

The double-transfected Madin-Darby canine kidney II (MDCKII) cell lines expressing both organic anion-transporting polypeptide 1B1 (OATP1B1/OATP-C/OATP2) or OATP1B3 (OATP8) in the basolateral membrane and MRP2 in the apical membrane, have been established as an in vitro model of hepatic vectorial transport of organic anions in humans (Cui et al., 2001; Sasaki et al., 2002). In this system, we can observe clear vectorial transport of bisubstrates for uptake and efflux transporters from the basal to the apical side compared with that in the opposite direction. The advantage of this double transfectant system is that it is able to evaluate the transport activities of apical transporters more sensitively compared with membrane vesicles. For example, with pravastatin (PRA), an anionic HMG-CoA reductase inhibitor, the ATP-dependent uptake is very small in human canalicular membrane vesicles (Niinuma et al., 1999), whereas the transcellular transport activity of PRA in OATP1B1/MRP2 double transfectant is large enough to observe its saturation kinetics (Sasaki et al., 2002).

In the present study, we constructed new double transfectants, expressing OATP1B1/MDR1 and OATP1B1/BCRP, and investigated the transcellular transport of organic anions to determine which transporters are involved in the biliary excretion. OATP1B1 is exclusively expressed in human liver and accepts many kinds of organic anions (Abe et al., 1999; Hsiang et al., 1999; Konig et al., 2000), and very recently, Hirano et al. (2004) showed that pitavastatin and EG are mainly taken up by OATP1B1 across the human basolateral membrane (Hirano et al., 2004). Accordingly, ligands can efficiently reach the efflux transporters from the intracellular compartment via OATP1B1, which makes this system useful for the characterization of the efflux transport of organic anions on the bile canalicular membranes. We investigated the transcellular transport of the following organic anions, EG and estrone-3-sulfate (ES), and HMG-CoA reductase inhibitors cerivastatin (CER) and PRA, to examine whether these compounds exhibited vectorial basal-to-apical transport in each double transfectant or not.

Materials and Methods

Materials. [^{3}H]EG (1.6 TBq/mmol) and [^{3}H]ES (2.2 TBq/mmol) were purchased from PerkinElmer Life and Analytical Sciences (Boston, MA). [^{3}H]CER (0.18 TBq/mmol) was synthesized by Hartmann Analytic GmbH (Braunschweig, Germany). [^{3}H]PRA (1.6 TBq/mmol) was kindly donated by Sankyo Co. Ltd. (Tokyo, Japan). Unlabeled CER was kindly donated by Bayer AG (Wuppertal, Germany). pEB6CAGMCS/SRZeo was kindly donated by Dr. Miwa (Tsukuba University, Tsukuba, Japan) (Tanaka et al., 1999). Parental MDCKII cells and MDCKII cells expressing human MRP2 (Evers et al., 1998) and MDR1 were kindly provided by Dr. Piet Borst (The Netherlands Cancer Institute, Amsterdam, The Netherlands). All other chemicals were commercially available and of reagent grade.

Construction of Plasmid Vector. Previously cloned human OATP1B1 cDNA in pcDNA3.1/Zeo (+) vector (Iwai et al., 2004) was subcloned into the NotI and XhoI sites of pEB6CAGMCS/SRZeo vector, which is an Epstein-Barr virus-based vector, and the subcloned gene was localized and replicated in the episome and not integrated into the genome of the host cells (Tanaka et al., 1999).

Cell Culture and Transfection of Expression Vector. Parental MDCKII cells and MDCKII cells expressing human MRP2 or MDR1 were cultured in Dulbecco's modified Eagle's medium (low glucose version) (Invitrogen, Carlsbad, CA) with 10% fetal bovine serum (Sigma-Aldrich, St. Louis, MO) and 1% antibiotic-antimycotic solution (Sigma-Aldrich) at 37°C under 5% CO_2. The transporter cDNA in the episomal expression vector was transfected into MDCKII cells using FuGENE6 reagent (Roche Diagnostics Co., Indianapolis, IN). At 50% confluence, cells on six-well plates were exposed to serum-free Dulbecco's modified Eagle's medium containing plasmid and FuGENE6 according to the manufacturer's instruction. At 6 h after the initiation of transfection, the plasmid-FuGENE6 solution was replaced with the normal culture medium. The transfected MDCKII cells were selected with Zeocin (700 μg/ml; Invitrogen).

Construction of Human BCRP-Expressing Cells. For constructing MDCKII cells expressing human BCRP, MDCKII cells were infected with recombinant adenoviruses containing human BCRP cDNA (Kondo et al., 2004) at 200 multiplicity of infection, 48 h prior to all experiments. The virus titer was determined as described previously (Kondo et al., 2004).

Western Blot Analysis. For Western blot analysis, crude membrane was prepared from MDCKII cells according to the method of the previous report (Gant et al., 1991). After the crude membrane was suspended in PBS, it was frozen in liquid N_2 and stored at −80°C until used. The protein concentrations in the crude membrane vesicles prepared from MDCKII cells were determined by the method of Lowry with bovine serum albumin as a standard. The membrane fraction was dissolved in 3× SDS sample buffer (New England Biolabs, Beverly, MA) with β-mercaptoethanol and loaded onto a 7% SDS-polyacrylamide electrophoresis gel with a 4.4% stacking gel. The molecular weight was determined using a prestained protein marker (New England Biolabs). Proteins were transferred electrophoretically to a polyvinylidene difluoride membrane (Pall, East Hills, NY) using a blotter (Trans-blot; Bio-Rad, Hercules, CA) at 15 V for 1 h. The membrane was blocked with Tris-buffered saline with 0.05% Tween 20 (TTBS) and 5% skimmed milk overnight at 4°C. After washing with TTBS, the membrane was incubated at room temperature in TTBS with 1000-fold diluted anti-OATP1B1 polyclonal antibody (Alpha Diagnostic International Inc., San Antonio, TX) for 1 h, 125-fold diluted monoclonal antibody against MRP2 (M_2III-6; Alexis Biochemicals, Gruenberg, Germany) for 2 h, 100-fold

diluted monoclonal antibody against MDR1 (C219; Signet Laboratories, Inc., Dedham, MA) for 1 h, or 200-fold diluted monoclonal antibody against BCRP (BXP-21; Kamiya Biomedical Company, Seattle, WA) for 2 h. For the detection of each transporter, the membrane was placed in contact with 2500-fold diluted donkey anti-rabbit (OATP1B1) or anti-mouse IgG (MRP2, MDR1, and BCRP) conjugated with the horseradish peroxidase (Amersham Biosciences Inc., Piscataway, NJ) for 1 h in TTBS. The band was detected using an ECL Plus Western blotting starter kit (Amersham Biosciences Inc.), and its intensity was quantified in a luminescent image analyzer (LAS-3000 mini; Fuji Film Corp., Tokyo, Japan).

Immunocytochemical Staining. For immunocytochemical staining, transfectants were plated at a density of 5×10^5 cells in 12-well plates, 96 h prior to the experiments. Sodium butyrate (5 mM) was added to the culture medium 1 day before the experiments. After fixation with methanol at −20°C for 10 min and permeabilization in 1% Triton X-100 in PBS at room temperature for 10 min, cells were incubated for 1 h at room temperature with 50-fold diluted anti-OATP1B1 rabbit serum, which was raised in rabbits against the 21 amino acids at the carboxyl terminus of the deduced OATP1B1 sequence (ESLNKNKHFVPSAGADSETHC), 40-fold diluted monoclonal antibody against MRP2 (M_2III-6), 40-fold diluted monoclonal antibody against MDR1 (C219), or 40-fold diluted monoclonal antibody against BCRP (BXP-21). Then, cells were washed with PBS three times and incubated for 1 h at room temperature with 250-fold diluted goat anti-rabbit IgG Alexa 488 (Molecular Probes Inc., Eugene, OR) for OATP1B1 or 250-fold diluted goat anti-mouse IgG Alexa 568 (Molecular Probes Inc.) for MRP2, MDR1, and BCRP. Nuclei were stained with 250-fold diluted TO-PRO-3 iodide (Molecular Probes Inc.). The localization was visualized by confocal laser microscopy (Zeiss LSM-510; Carl Zeiss Inc., Thornwood, NY).

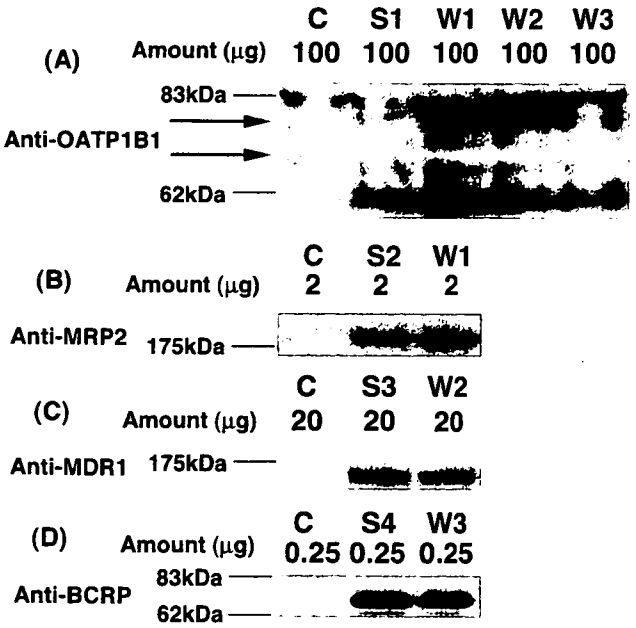

Fig. 1. Western blot analysis of OATP1B1, MRP2, MDR1, and BCRP in crude membrane vesicles obtained from MDCKII transfectants. Crude membrane prepared from MDCKII transfectants was separated by SDS-polyacrylamide gel electrophoresis. OATP1B1 was detected using polyclonal antibody against the carboxyl terminus of human OATP1B1 (A). MRP2, MDR1, and BCRP were detected using monoclonal antibody against the linker region of human MRP2 (B), MDR1 (C), and BCRP (D), respectively. The amount of protein applied to each lane in panel (A), (B), (C), and (D) was 100, 2, 20, and 0.25 μg. C, S1–4, W1–3 represent vector-transfected MDCKII cells, single-transfected cells (S1, OATP1B1; S2, MRP2; S3, MDR1; S4, BCRP), and double-transfected cells (W1, OATP1B1/MRP2; W2, OATP1B1/MDR1; W3, OATP1B1/BCRP). Arrows represent the specific bands for OATP1B1.

Transcellular Transport Study. The transcellular transport study was performed as reported previously (Sasaki et al., 2002). Briefly, MDCKII cells were grown on Transwell membrane inserts (6.5-mm diameter, 0.4-μm pore size; Corning Coster, Bodenheim, Germany) at confluence for 3 days, and the expression level of transporters was induced with 5 mM sodium butyrate for 24 h before the transport study. Cells were first washed with Krebs-Henseleit buffer (118 mM NaCl, 23.8 mM $NaHCO_3$, 4.83 mM KCl, 0.96 mM KH_2PO_4, 1.20 mM $MgSO_4$, 12.5 mM HEPES, 5.0 mM glucose, and 1.53 mM $CaCl_2$ adjusted to pH 7.4) at 37°C or 4°C. Subsequently, radiolabeled substrates were added in Krebs-Henseleit buffer either to the apical compartments (250 μl) or to the basolateral compartments (1 ml). After a designated period, the radioactivity in 100-μl medium in the opposite compartments was measured in a liquid scintillation counter (LS 6000SE; Beckman Coulter, Fullerton, CA). At the end of the experiments, the cells were washed three times with 1.5 ml of ice-cold Krebs-Henseleit buffer and solubilized in 500 μl of 0.2 M NaOH. After addition of 100 μl of 1 M HCl, 450-μl aliquots were transferred to the liquid scintillation counter for determination of radioactivity. Fifty-microliter aliquots of cell lysate were used to determine protein concentrations by the method of Lowry with bovine serum albumin as a standard.

Calculation of the Transport Activities of Recombinant MRP2, MDR1, and BCRP across the Double Transfectants. The apparent efflux clearance across the apical membrane ($PS_{apical,\ x°C}$) at each temperature (37°C or 4°C) was calculated by dividing the steady-state velocity for the transcellular transport ($V_{transcellular,\ x°C}$) of compounds determined over 2 h by the cellular concentration ($C_{cell,\ x°C}$) of the compounds determined at the end of the experiments (over 2 h) at each temperature (37°C or 4°C). The steady-state velocity for the transcellular transport was calculated by dividing the basal-to-apical transport amount at 2 h ($X_{x°C}$) when the steady-state condition was maintained (see *Results*) by 120 min. Then, to evaluate the activity of transporter-mediated transcellular transport, $PS_{apical,\ 4°C}$, the clearance at 4°C (at this temperature the active transport systems are not functional), was subtracted from $PS_{apical,\ 37°C}$. Moreover, since some endogenous efflux transporters have been reported to be expressed in MDCKII cells (Goh et al., 2002; Guo et al., 2002), the specific transport activity across the apical

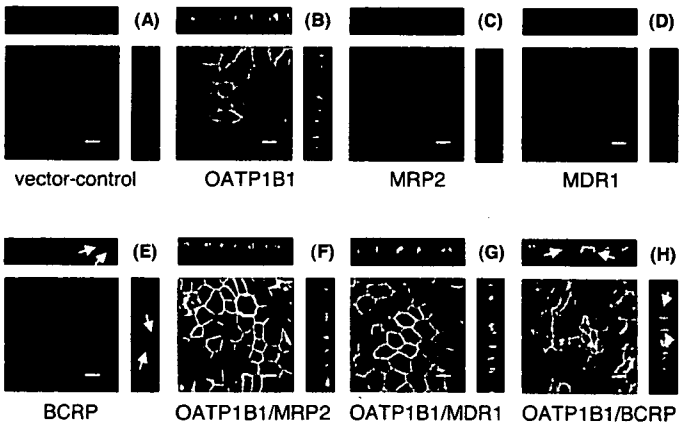

Fig. 2. Immunolocalization of recombinant OATP1B1, MRP2, MDR1, and BCRP in MDCKII cells. MDCKII cells transfected with empty vector (A), OATP1B1 (B), MRP2 (C), MDR1 (D), BCRP (E), both OATP1B1 and MRP2 (F), both OATP1B1 and MDR1 (G), and both OATP1B1 and BCRP (H) were stained with polyclonal antiserum against human OATP1B1 (green fluorescence, A–H), monoclonal antibody against human MRP2 (red fluorescence, A–C, and F), human MDR1 (red fluorescence, A, B, D, and G) and human BCRP (red fluorescence, A, B, E, and H). A and B show the staining with antiserum against human OATP1B1 and MDR1. The results were similar to the staining with antiserum against human OATP1B1/MRP2 or OATP1B1/BCRP (data not shown). Nuclei were stained with TO-PRO-3 (blue fluorescence). Pictures are single optical sections (x,y) (center) with xz (top) and yz (right) projections, respectively. Bar = 20 μm.

membrane (TA) mediated by exogenously expressed efflux transporters was calculated by subtracting the transporter-mediated clearance in each double transfectant from that in the single transfectant expressing only OATP1B1, as described in the following equations:

$$PS_{apical,x°C} = \frac{V_{transcellular,x°C}}{C_{cell,x°C}} \quad (1)$$

$$TA = (PS_{apical,37°C,double} - PS_{apical,4°C,double}) - (PS_{apical,37°C,single} - PS_{apical,4°C,single}) \quad (2)$$

Results

Expression of Human OATP1B1, MRP2, MDR1, and BCRP in MDCKII Cells. The expression of OATP1B1, MRP2, MDR1, and BCRP in double transfectants was confirmed by Western blot analysis (Fig. 1). Two major bands, which appeared at 83 and 62 kDa, could be detected in all kinds of OATP1B1-transfected cells (Fig. 1A), as shown previously (Konig et al., 2000). We were able to clearly detect human MRP2, MDR1, and BCRP with apparent molecular masses of about 190, 170, and 70 kDa (Fig. 1, B–D). The band also reacted slightly with the C219 antibody in wild-type MDCKII cells (Fig. 1C).

Localization of Recombinant Human OATP1B1, MRP2, MDR1, and BCRP. The cellular localization of the recombinant transporters in each transfectant was confirmed by confocal laser scanning microscopy. OATP1B1 was localized in the basolateral membrane (Fig. 2, B and F–H), whereas MRP2 and MDR1 were localized in the apical membrane (Fig. 2, C, D, F, and G). BCRP was mainly detected in the apical membrane, but part of the BCRP was also detected in the basolateral membrane (Fig. 2, E and H).

Transcellular Transport of EG, ES, CER, and PRA across the MDCKII Cell Monolayer. Transcellular transport of conjugated steroids EG and ES across the MDCKII monolayer was determined. As shown in Fig. 3, F–H, the basal-to-apical transport of EG was approximately 17, 6.7, and 8.8 times higher than that in the opposite direction in OATP1B1/MRP2, OATP1B1/MDR1, and OATP1B1/BCRP double transfectants, respectively, whereas the basal-to-apical flux of EG across the OATP1B1-expressing MDCKII cells was approximately 2.3 times higher than that in the opposite direction (Fig. 3B). A symmetrical flux of EG was observed across the control and MRP2-, MDR1-, and BCRP-expressing MDCKII cells (Fig. 3, A and C–E). For ES, the basal-to-apical transport was approximately 2.2-, 3.0-, 10-, and 41-fold higher than that in the opposite direction in OATP1B1-, OATP1B1/MRP2-, OATP1B1/MDR1-, and OATP1B1/BCRP-expressing MDCKII cells, respectively (Fig. 4 B and F–H). On the other hand, a symmetrical flux of ES was observed across the control and MRP2-, MDR1-, and BCRP-expressing MDCKII cells (Fig. 4, A and C–E). Transcellular transport of two kinds of HMG-CoA reductase inhibitors, CER and PRA, was also determined in the MDCKII transfectants. As shown in

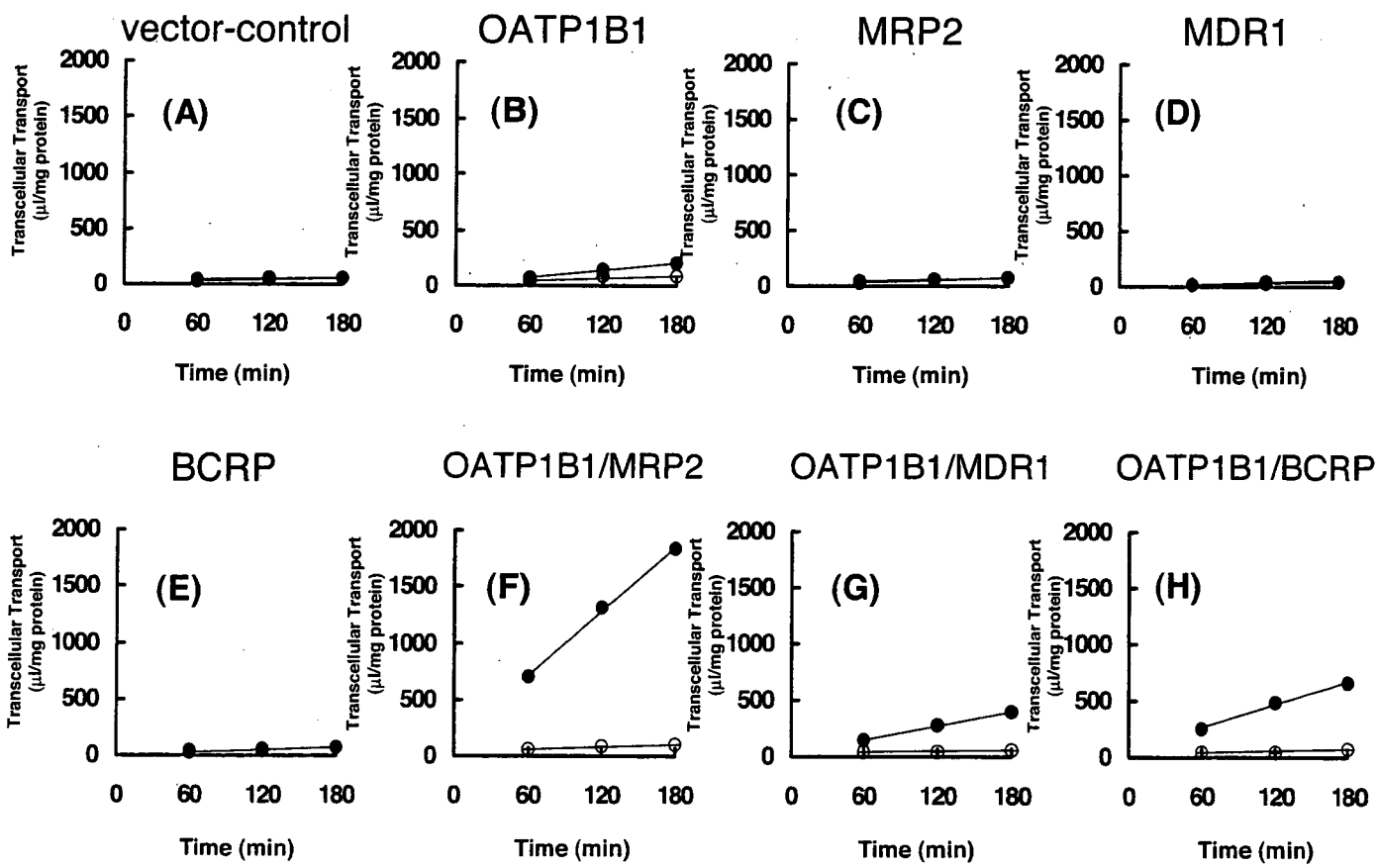

Fig. 3. Time profiles for the transcellular transport of [^{3}H]EG across MDCKII monolayers. Transcellular transport of [^{3}H]EG (0.5 μM) across MDCKII monolayers expressing OATP1B1 (B), MRP2 (C), MDR1 (D), BCRP (E), both OATP1B1 and MRP2 (F), both OATP1B1 and MDR1 (G), and both OATP1B1 and BCRP (H) was compared with that across the control MDCKII monolayer (A). Open and closed circles represent the transcellular transport in the apical-to-basal and basal-to-apical direction, respectively. Each point and vertical bar represents the mean ± S.E. of three determinations. Where vertical bars are not shown, the S.E. was contained within the limits of the symbol.

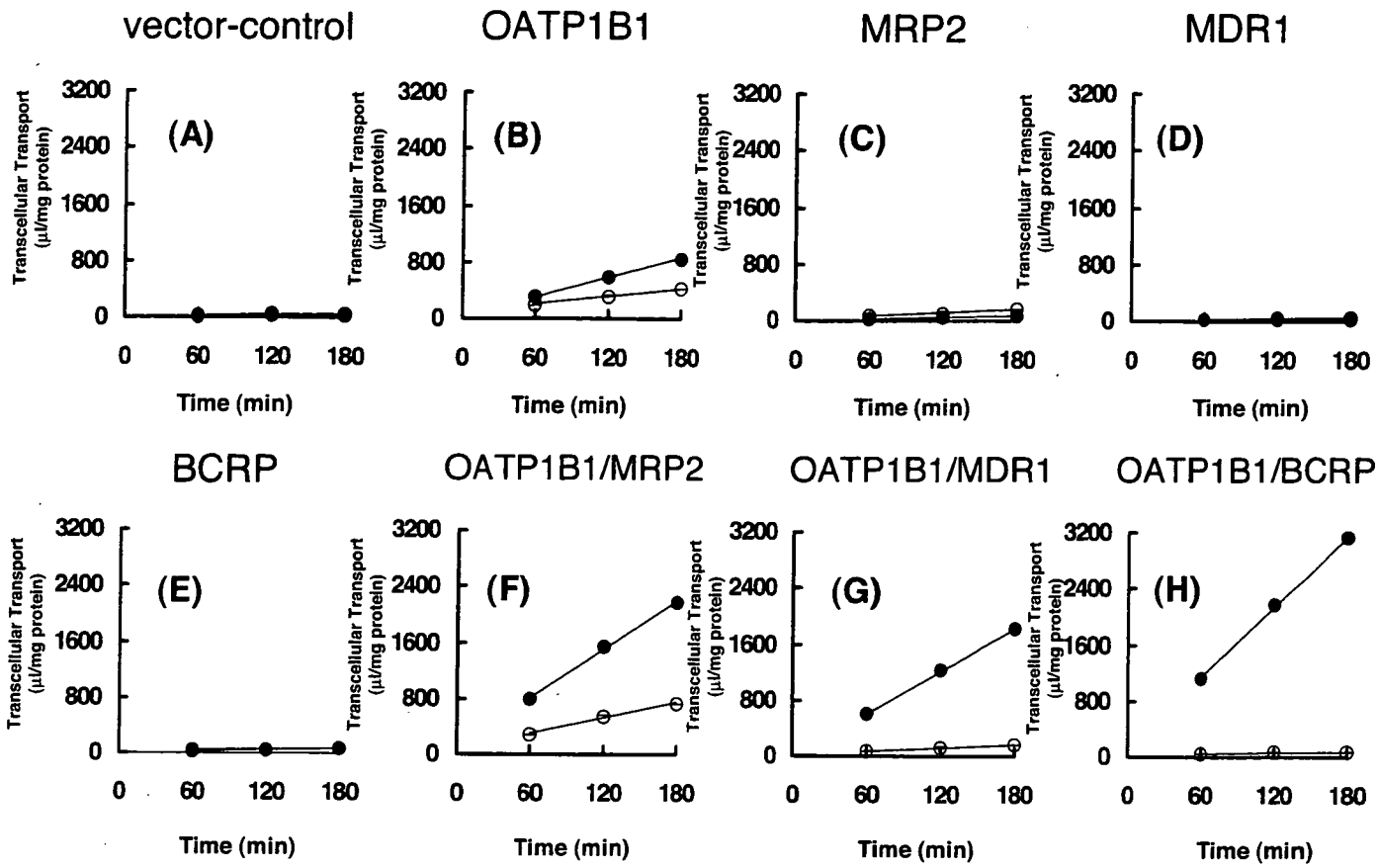

Fig. 4. Time profiles for the transcellular transport of [^{3}H]ES across MDCKII monolayers. Transcellular transport of [^{3}H]ES (0.5 μM) across MDCKII monolayers expressing OATP1B1 (B), MRP2 (C), MDR1 (D), BCRP (E), both OATP1B1 and MRP2 (F), both OATP1B1 and MDR1 (G), and both OATP1B1 and BCRP (H) was compared with that across the control MDCKII monolayer (A). Open and closed circles represent the transcellular transport in the apical-to-basal and basal-to-apical direction, respectively. Each point and vertical bar represents the mean ± S.E. of three determinations. Where vertical bars are not shown, the S.E. was contained within the limits of the symbol.

Fig. 5, F–H, the basal-to-apical transport of CER was 3.8, 6.3, and 3.1 times higher than that in the opposite direction in OATP1B1/MRP2-, OATP1B1/MDR1-, and OATP1B1/BCRP-expressing MDCKII cells, respectively, whereas a symmetrical flux of CER was observed across the control and all of the single transfectants (Fig. 5, A–E). On the other hand, the basal-to-apical flux of PRA was significantly 3.3-fold higher than that in the opposite direction only in OATP1B1/MRP2-expressing MDCKII cells (Fig. 6F). However, in the other cell lines, the ratio of the basal-to-apical flux to that in the opposite direction was less than two (Fig. 6, A–E, G, and H).

Calculation of the Transport Activities of Recombinant MRP2, MDR1, and BCRP across the Apical Membrane of the Double Transfectants. To estimate quantitatively the transport activity by the recombinant transporters across the apical membrane, the clearance to the apical compartment from cells (TA) was determined as described under *Materials and Methods*. The clearance for EG was 3.56 ± 0.07, 0.420 ± 0.026, and 0.383 ± 0.059 in OATP1B1/MRP2-, OATP1B1/MDR1-, and OATP1B1/BCRP-expressing MDCKII cells, respectively (Fig. 7A). The clearance for ES was 0.268 ± 0.013, 0.351 ± 0.011, and 2.31 ± 0.02 μl/min/mg protein in OATP1B1/MRP2-, OATP1B1/MDR1-, and OATP1B1/BCRP-expressing MDCKII cells, respectively (Fig. 7B). Regarding the statins, the clearance for CER was 0.612 ± 0.039, 0.669 ± 0.062, and 0.201 ± 0.007 μl/min/mg protein in OATP1B1/MRP2-, OATP1B1/MDR1-, and OATP1B1/BCRP-expressing MDCKII cells, respectively (Fig. 7C), whereas the clearance for PRA was 3.75 ± 0.112, 0.393 ± 0.097, and 0.194 ± 0.087 μl/min/mg protein, respectively (Fig. 7D).

Discussion

In the present study, we constructed new double transfectants expressing OATP1B1/MDR1 and OATP1B1/BCRP and observed the transcellular transport of four organic anions, EG and ES (steroid conjugates) and CER and PRA (HMG-CoA reductase inhibitors), to examine the substrate specificities and relative transport activities of the efflux transporters MDR1, MRP2, and BCRP. Western blot and immunocytochemical analyses revealed that OATP1B1, MRP2, and MDR1 were expressed in MDCKII cells and localized correctly on the basolateral (OATP1B1) and apical membranes (MRP2 and MDR1), respectively, but BCRP was localized mainly on the apical membrane and only partially on the basolateral membrane (Fig. 2). On the other hand, we could clearly observe significant basal-to-apical vectorial transport of organic anions in OATP1B1/BCRP double-transfected cells (Figs. 3–5), suggesting that minor expression of BCRP on the basal side does not affect the observation of the vectorial transport of substrates with our double transfectant, although basal-to-apical transport was thought to be partly inhibited by the basal expression of BCRP.

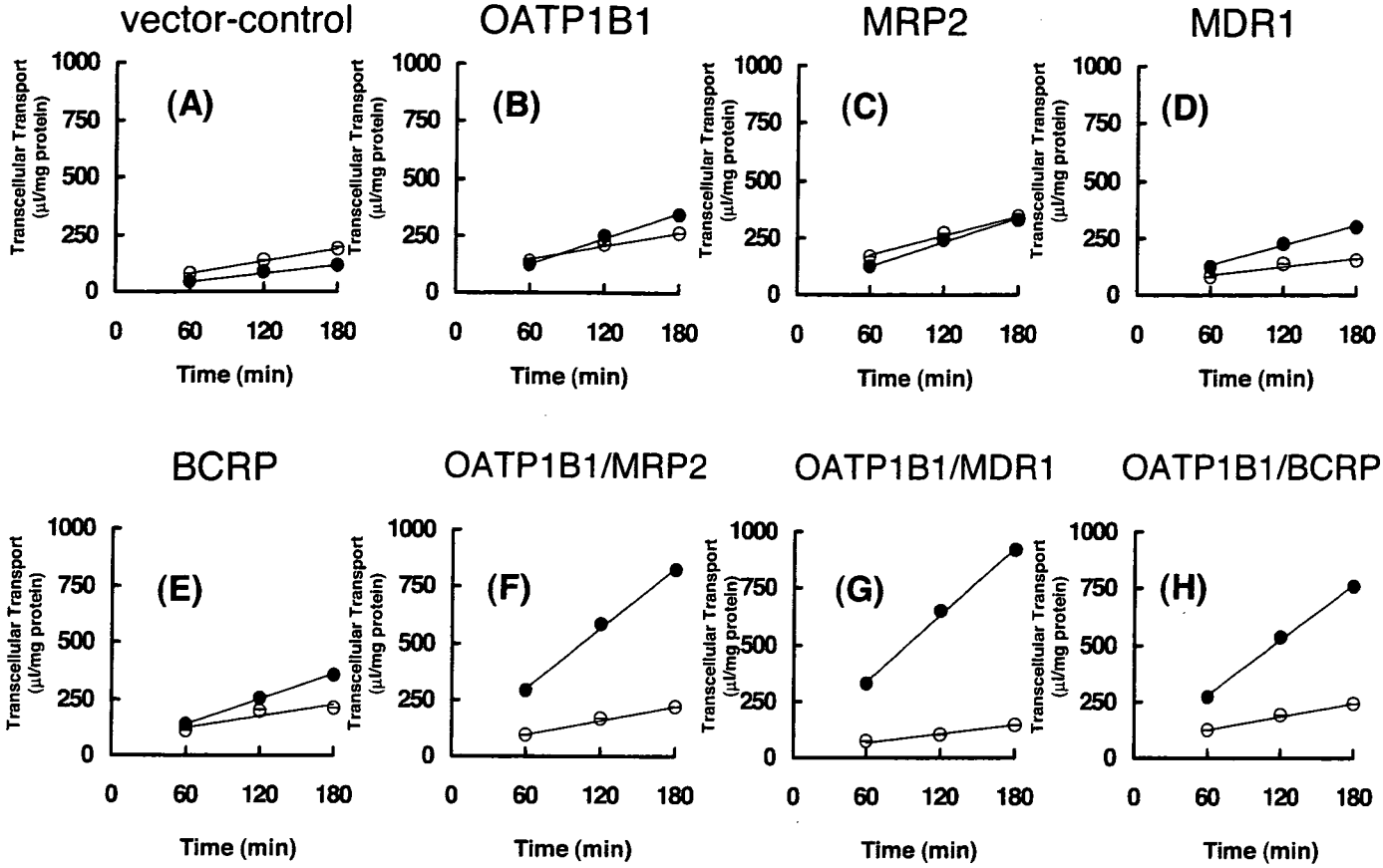

Fig. 5. Time profiles for the transcellular transport of [^{3}H]CER across MDCKII monolayers. Transcellular transport of [^{3}H]CER (0.5 μM) across MDCKII monolayers expressing OATP1B1 (B), MRP2 (C), MDR1 (D), BCRP (E), both OATP1B1 and MRP2 (F), both OATP1B1 and MDR1 (G), and both OATP1B1 and BCRP (H) was compared with that across the control MDCKII monolayer (A). Open and closed circles represent the transcellular transport in the apical-to-basal and basal-to-apical direction, respectively. Each point and vertical bar represents the mean ± S.E. of three determinations. Where vertical bars are not shown, the S.E. was contained within the limits of the symbol.

Then, we performed a transcellular transport study involving four kinds of organic anions using three types of double transfectants (Figs. 3–6). The double transfectant is a useful tool for identifying bisubstrates for uptake and efflux transporters and suitable for high throughput screening (Sasaki et al., 2002). Another advantage of this system is to characterize the function of efflux transporters easily because some compounds cannot access the efflux transporter from the intracellular compartment without the aid of uptake transporters. In this study, all test compounds are known to be substrates of OATP1B1 (Abe et al., 1999; Hsiang et al., 1999; Shitara et al., 2003), and compounds can interact with efflux transporters efficiently.

The transcellular transport clearance (PS_{trans}) was determined by both uptake and efflux clearance as shown in eq. 3.

$$PS_{trans} = PS_{uptake} \times \frac{PS_{apical}}{PS_{apical} + PS_{basal}} \quad (3)$$

where PS_{uptake} represents the uptake clearance from the basal side to the cell, and PS_{apical} and PS_{basal} represent the efflux clearance from the cell to the apical side and to the basal side, respectively. If PS_{apical} is much larger than PS_{basal}, which is a typical case when the efflux transporter can recognize the substrate, PS_{trans} is approximately equal to PS_{uptake}, which is determined by the function of OATP1B1. So, the transcellular transport clearance does not always reflect the function of the efflux transporter. Therefore, to estimate the relative clearance of each efflux transporter, we calculated the PS_{apical} values by transcellular clearance from the basal to apical side normalized by the intracellular ligand concentration (Fig. 7).

EG was efficiently transported from the basolateral to apical side in all these double transfectants (Fig. 3), and the efflux clearance of MRP2 was much higher than that of MDR1 and BCRP (Fig. 7A). We previously reported that Mrp2 is predominantly involved in the biliary excretion of EG in rats (Morikawa et al., 2000). It has also been reported that EG is a substrate of human MDR1 and BCRP (Huang et al., 1998; Chen et al., 2003).

We were also able to observe the vectorial transcellular transport of ES in all kinds of double transfectants, and efflux transporters were able to enhance the basal-to-apical transport of ES compared with the transport in OATP1B1 single transfectant. BCRP showed the highest efflux clearance of ES among the three transporters (Fig. 7B). Suzuki et al. (2003) reported that BCRP preferentially transports sulfated conjugates (Suzuki et al., 2003), and our results suggest that the sulfate-conjugated steroid ES could be transported preferentially by BCRP in our double transfectants compared with MDR1 and MRP2. This result agrees with the previous report demonstrating that the biliary excretion of the sulfated steroid E3040 sulfate was maintained even in EHBR, an Mrp2-deficient rat (Takenaka et al., 1995)

HMG-CoA reductase inhibitors (statins) are efficiently

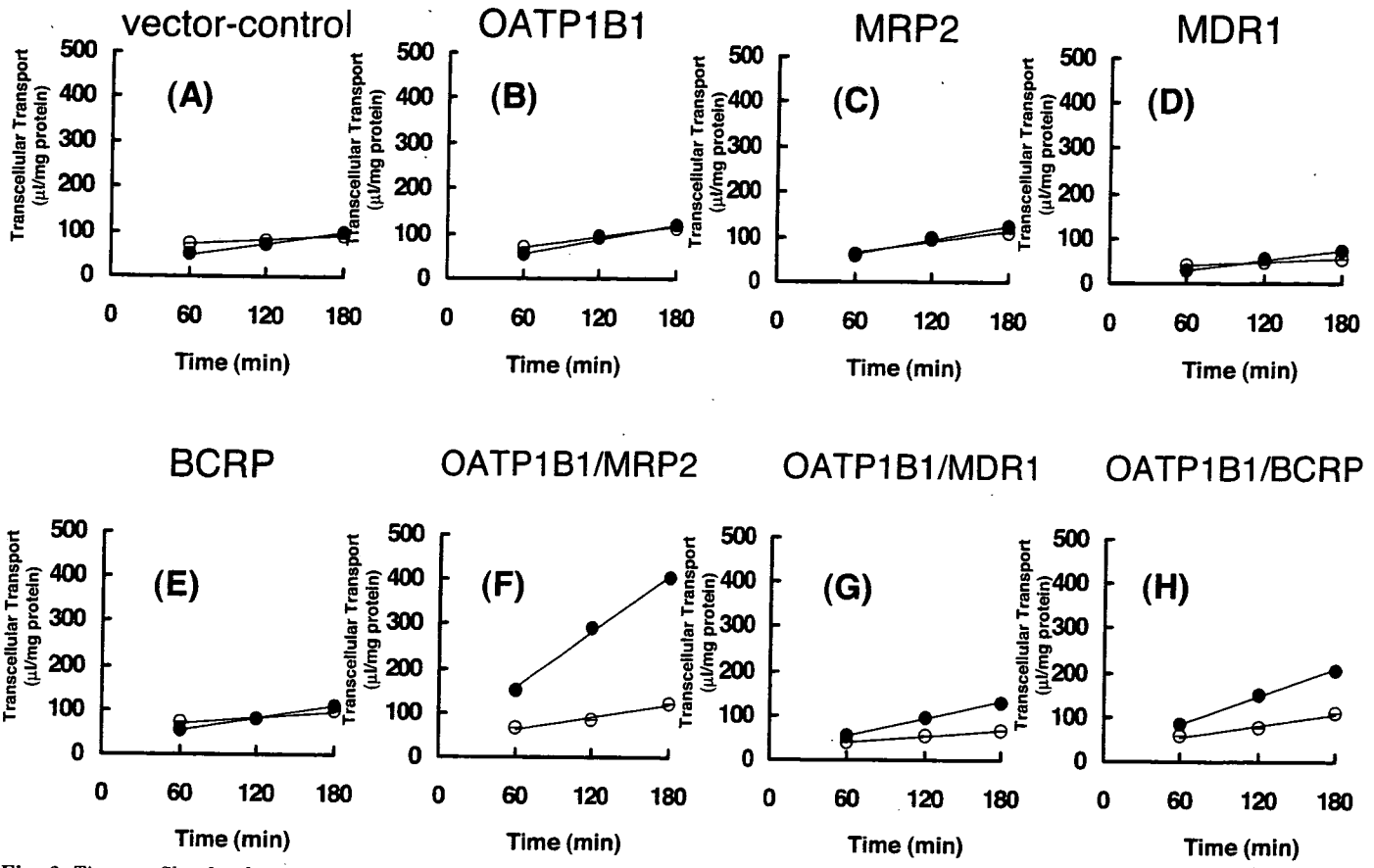

Fig. 6. Time profiles for the transcellular transport of [^{3}H]PRA across MDCKII monolayers. Transcellular transport of [^{3}H]PRA (0.5 μM) across MDCKII monolayers expressing OATP1B1 (B), MRP2 (C), MDR1 (D), BCRP (E), both OATP1B1 and MRP2 (F), both OATP1B1 and MDR1 (G), and both OATP1B1 and BCRP (H) was compared with that across the control MDCKII monolayer (A). Open and closed circles represent the transcellular transport in the apical-to-basal and basal-to-apical direction, respectively. Each point and vertical bar represents the mean ± S.E. of three determinations. Where vertical bars are not shown, the S.E. was contained within the limits of the symbol.

taken up into the liver, where cholesterol is synthesized (Igel et al., 2001). Among these statins, PRA, CER, pitavastatin, and rosuvastatin are reported to be substrates of OATP1B1 (Brown et al., 2001; Nakai et al., 2001; Sasaki et al., 2002; Shitara et al., 2003; Hirano et al., 2004). The basal-to-apical flux of CER was significantly higher than that in the opposite direction in all the double transfectants compared with the OATP1B1 single transfectant (Fig. 5), suggesting that CER is a substrate of MRP2, MDR1, and BCRP. A previous report has demonstrated that the transcellular transport of CER from the basal to apical side across the MDR1-expressed MDCK monolayer was significantly greater than that in the opposite direction (Hirai et al., 2001). We were also able to obtain reproducible results in the MDR1 single transfectant (Fig. 5D). On the other hand, the ratio of the basal-to-apical flux to the apical-to-basal flux of PRA was significantly high only in the OATP1B1/MRP2 double transfectant, whereas the flux ratio was only slightly raised in OATP1B1/MDR1 and OATP1B1/BCRP transfectants (Fig. 6). Previous reports have suggested that the biliary excretion of PRA was mostly mediated by rat Mrp2 (Yamazaki et al., 1997). Interestingly, the relative activities of each transporter for PRA were very similar to those for EG, and previous reports have demonstrated that Mrp2 is responsible for the biliary excretion of both PRA and EG in rats, suggesting that PRA and EG may share the same route of biliary excretion, possibly MRP2. However, considering the reported species differences in the expression level of transporters (Ishizuka et al., 1999), we cannot easily estimate the relative contribution of each efflux transporter from our own data alone and will need further analyses in which we compare the expression level of apically localized transporters in double transfectants and human liver accurately. In our expression system, we observed a low degree of MDR1-mediated transport of PRA. Some reports have shown that PRA does not interact with MDR1 using a cell system (Hirai et al., 2001; Wang et al., 2001; Sakaeda et al., 2002). However, it is possible that the intracellular concentration of PRA was too low for them to detect MDR1-mediated efflux of PRA because PRA cannot cross the basal membrane in the MDR1 single transfectant.

In conclusion, we have constructed new double-transfected cell lines and determined the substrate specificities and relative transport activities of MRP2, MDR1, and BCRP for organic anions. Vectorial transport of EG, ES, CER, and PRA from the basal to apical side was observed in OATP1B1/MRP2-, OATP1B1/MDR1-, and OATP1B1/BCRP-expressing cells. The transport activities of EG and PRA by MRP2 were the highest, considering that MRP2 may be mainly involved in the transport of EG and PRA in humans as well as rodents. In the case of ES, BCRP may play an important role in the biliary excretion. It is interesting that two kinds of structurally related HMG-CoA reductase inhibitors, PRA and CER, showed different relative contributions from each transporter as far as biliary excretion is concerned. This system is

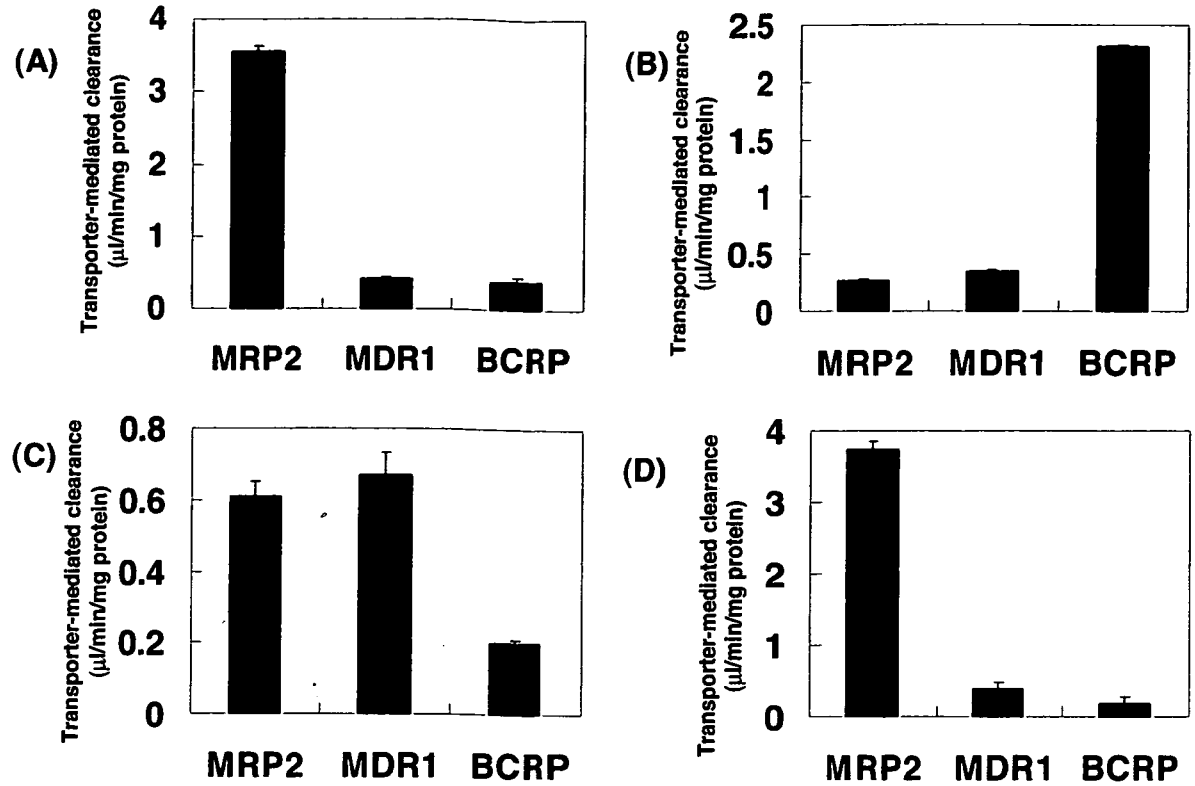

Fig. 7. Estimation of transporter-mediated efflux activity (TA) for the MRP2, MDR1, and BCRP transfectants. The TA values for EG (A), ES (B), CER (C), and PRA (D) were determined as described under *Materials and Methods*. Values are given as the mean ± S.E. of three determinations.

useful for the determination of the substrate specificities of hepatic efflux transporters for hydrophilic organic anions, which cannot easily be extruded from the cellular membrane. We can also determine the substrate dependence of the relative contribution of each transporter using this double-transfected cell system.

Acknowledgments

We thank Dr. Piet Borst (The Netherlands Cancer Institutes) for providing the MDCKII cells expressing MRP2 or MDR1, Sankyo Co. (Tokyo, Japan) for providing labeled and unlabeled pravastatin, Bayer HealthCare AG (Wuppertal, Germany) for unlabeled cerivastatin, and Dr. Yoshihiro Miwa (Tsukuba University, Japan) for pEB6CAGMCS/SRZeo vector.

References

Abe T, Kakyo M, Tokui T, Nakagomi R, Nishio T, Nakai D, Nomura H, Unno M, Suzuki M, Naitoh T, et al. (1999) Identification of a novel gene family encoding human liver-specific organic anion transporter LST-1. *J Biol Chem* **274**:17159–17163.

Brown CDA, Windass A, Bleasby K, and Lauffart B (2001) Rosuvastatin is a high affinity substrate of hepatic organic anion transporter OATP-C. *Atherosclerosis Suppl* **2**:90.

Chen ZS, Robey RW, Belinsky MG, Shchaveleva I, Ren XQ, Sugimoto Y, Ross DD, Bates SE, and Kruh GD (2003) Transport of methotrexate, methotrexate polyglutamates and 17beta-estradiol 17-(beta-D-glucuronide) by ABCG2: effects of acquired mutations at R482 on methotrexate transport. *Cancer Res* **63**:4048–4054.

Cui Y, Konig J, and Keppler D (2001) Vectorial transport by double-transfected cells expressing the human uptake transporter SLC21A8 and the apical export pump ABCC2. *Mol Pharmacol* **60**:934–943.

Cvetkovic M, Leake B, Fromm MF, Wilkinson GR, and Kim RB (1999) OATP and P-glycoprotein transporters mediate the cellular uptake and excretion of fexofenadine. *Drug Metab Dispos* **27**:866–871.

Evers R, Kool M, van Deemter L, Janssen H, Calafat J, Oomen LC, Paulusma CC, Oude Elferink RP, Baas F, Schinkel AH, and Borst P (1998) Drug export activity of the human canalicular multispecific organic anion transporter in polarized kidney MDCK cells expressing cMOAT (MRP2) cDNA. *J Clin Investig* **101**:1310–1319.

Gant TW, Silverman JA, Bisgaard HC, Burt RK, Marino PA, and Thorgeirsson SS (1991) Regulation of 2-acetylaminofluorene-and 3-methylcholanthrene–mediated induction of multidrug resistance and cytochrome P450IA gene family expression in primary hepatocyte cultures and rat liver. *Mol Carcinog* **4**:499–509.

Goh LB, Spears KJ, Yao D, Ayrton A, Morgan P, Roland Wolf C, and Friedberg T (2002) Endogenous drug transporters in in vitro and in vivo models for the prediction of drug disposition in man. *Biochem Pharmacol* **64**:1569–1578.

Guo A, Marinaro W, Hu P, and Sinko PJ (2002) Delineating the contribution of secretory transporters in the efflux of etoposide using Madin-Darby canine kidney (MDCK) cells overexpressing P-glycoprotein (Pgp), multidrug resistance-associated protein (MRP1) and canalicular multispecific organic anion transporter (cMOAT). *Drug Metab Dispos* **30**:457–463.

Hirai S, Jacobson W, Djuvo S, Benet LZ, and Christians U (2001) Comparison of the P-glycoprotein-mediated transport of HMG-CoA reductase inhibitors across MDCK-MDR1 cell monolayers (Abstract). *AAPS Pharm Sci* **3**:online.

Hirano M, Maeda K, Shitara Y, and Sugiyama Y (2004) Contribution of OATP2 (OATP1B1) and OATP8 (OATP1B3) to the hepatic uptake of pitavastatin in humans. *J Pharmacol Exp Ther* **311**:139–146.

Hsiang B, Zhu Y, Wang Z, Wu Y, Sasseville V, Yang WP, and Kirchgessner TG (1999) A novel human hepatic organic anion transporting polypeptide (OATP2). Identification of a liver-specific human organic anion transporting polypeptide and identification of rat and human hydroxymethylglutaryl-CoA reductase inhibitor transporters. *J Biol Chem* **274**:37161–37168.

Huang L, Hoffman T, and Vore M (1998) Adenosine triphosphate-dependent transport of estradiol-17beta(beta-D-glucuronide) in membrane vesicles by MDR1 expressed in insect cells. *Hepatology* **28**:1371–1377.

Igel M, Sudhop T, and von Bergmann K (2001) Metabolism and drug interactions of 3-hydroxy-3-methylglutaryl coenzyme A-reductase inhibitors (statins). *Eur J Clin Pharmacol* **57**:357–364.

Ishizuka H, Konno K, Shiina T, Naganuma H, Nishimura K, Ito K, Suzuki H, and Sugiyama Y (1999) Species differences in the transport activity for organic anions across the bile canalicular membrane. *J Pharmacol Exp Ther* **290**:1324–1330.

Iwai M, Suzuki H, Ieiri I, Otsubo K, and Sugiyama Y (2004) Functional analysis of single nucleotide polymorphisms of hepatic organic anion transporter OATP1B1 (OATP-C). *Pharmacogenetics* **14**:749–757.

Kondo C, Suzuki H, Itoda M, Ozawa S, Sawada J, Kobayashi D, Ieiri I, Mine K, Ohtsubo K, and Sugiyama Y (2004) Functional analysis of SNP variants of BCRP/ABCG2. *Pharm Res (NY)* **21**:1895–1903.

Konig J, Cui Y, Nies AT, and Keppler D (2000) A novel human organic anion transporting polypeptide localized to the basolateral hepatocyte membrane. *Am J Physiol Gastrointest Liver Physiol* **278**:G156–G164.

Konig J, Nies AT, Cui Y, Leier I, and Keppler D (1999) Conjugate export pumps of the multidrug resistance protein (MRP) family: localization, substrate specificity and MRP2-mediated drug resistance. *Biochim Biophys Acta* **1461**:377–394.

Lowry OH, Rosebrough NJ, Farr AL, and Randall RJ (1951) Protein measurement with folin phenol reagent. *J Biol Chem* **193**:265–267.

Maliepaard M, Scheffer GL, Faneyte IF, van Gastelen MA, Pijnenborg AC, Schinkel AH, van De Vijver MJ, Scheper RJ, and Schellens JH (2001) Subcellular localiza-

tion and distribution of the breast cancer resistance protein transporter in normal human tissues. *Cancer Res* **61**:3458–3464.
Morikawa A, Goto Y, Suzuki H, Hirohashi T, and Sugiyama Y (2000) Biliary excretion of 17beta-estradiol 17beta-D-glucuronide is predominantly mediated by cMOAT/MRP2. *Pharm Res (NY)* **17**:546–552.
Nakai D, Nakagomi R, Furuta Y, Tokui T, Abe T, Ikeda T, and Nishimura K (2001) Human liver-specific organic anion transporter, LST-1, mediates uptake of pravastatin by human hepatocytes. *J Pharmacol Exp Ther* **297**:861–867.
Niinuma K, Kato Y, Suzuki H, Tyson CA, Weizer V, Dabbs JE, Froehlich R, Green CE, and Sugiyama Y (1999) Primary active transport of organic anions on bile canalicular membrane in humans. *Am J Physiol* **276**:G1153–G1164.
Sakaeda T, Takara K, Kakumoto M, Ohmoto N, Nakamura T, Iwaki K, Tanigawara Y, and Okumura K (2002) Simvastatin and lovastatin, but not pravastatin, interact with MDR1. *J Pharm Pharmacol* **54**:419–423.
Sasaki M, Suzuki H, Ito K, Abe T, and Sugiyama Y (2002) Transcellular transport of organic anions across a double-transfected Madin-Darby canine kidney II cell monolayer expressing both human organic anion-transporting polypeptide (OATP2/SLC21A6) and multidrug resistance-associated protein 2 (MRP2/ABCC2). *J Biol Chem* **277**:6497–6503.
Shimamura H, Suzuki H, Hanano M, Suzuki A, Tagaya O, Horie T, and Sugiyama Y (1994) Multiple systems for the biliary excretion of organic anions in rats: liquiritigenin conjugates as model compounds. *J Pharmacol Exp Ther* **271**:370–378.
Shitara Y, Itoh T, Sato H, Li AP, and Sugiyama Y (2003) Inhibition of transporter-mediated hepatic uptake as a mechanism for drug-drug interaction between cerivastatin and cyclosporin A. *J Pharmacol Exp Ther* **304**:610–616.
Suzuki H and Sugiyama Y (1998) Excretion of GSSG and glutathione conjugates mediated by MRP1 and cMOAT/MRP2. *Semin Liver Dis* **18**:359–376.
Suzuki M, Suzuki H, Sugimoto Y, and Sugiyama Y (2003) ABCG2 transports sulfated conjugates of steroids and xenobiotics. *J Biol Chem* **278**:22644–22649.
Takenaka O, Horie T, Suzuki H, and Sugiyama Y (1995) Different biliary excretion systems for glucuronide and sulfate of a model compound; study using Eisai hyperbilirubinemic rats. *J Pharmacol Exp Ther* **274**:1362–1369.
Tanaka J, Miwa Y, Miyoshi K, Ueno A, and Inoue H (1999) Construction of Epstein-Barr virus-based expression vector containing mini-oriP. *Biochem Biophys Res Commun* **264**:938–943.
Tanigawara Y (2000) Role of P-glycoprotein in drug disposition. *Ther Drug Monit* **22**:137–140.
Thiebaut F, Tsuruo T, Hamada H, Gottesman MM, Pastan I, and Willingham MC (1987) Cellular localization of the multidrug-resistance gene product P-glycoprotein in normal human tissues. *Proc Natl Acad Sci USA* **84**:7735–7738.
Varadi A, Szakacs G, Bakos E, and Sarkadi B (2002) P glycoprotein and the mechanism of multidrug resistance. *Novartis Found Symp* **243**:54–65.
Wang E, Casciano CN, Clement RP, and Johnson WW (2001) HMG-CoA reductase inhibitors (statins) characterized as direct inhibitors of P-glycoprotein. *Pharm Res (NY)* **18**:800–806.
Yamazaki M, Akiyama S, Ni'inuma K, Nishigaki R, and Sugiyama Y (1997) Biliary excretion of pravastatin in rats: contribution of the excretion pathway mediated by canalicular multispecific organic anion transporter. *Drug Metab Dispos* **25**:1123–1129.

Address correspondence to: Dr. Yuichi Sugiyama, Department of Molecular Pharmacokinetics, Graduate School of Pharmaceutical Sciences, The University of Tokyo, 7-3-1 Hongo, Bunkyo-ku, Tokyo 113-0033, Japan. E-mail: sugiyama@mol.f.u-tokyo.ac.jp

Am J Physiol Gastrointest Liver Physiol 288: G159–G167, 2005.
First published August 5, 2004; doi:10.1152/ajpgi.00360.2003.

Vectorial transport of bile salts across MDCK cells expressing both rat Na^+-taurocholate cotransporting polypeptide and rat bile salt export pump

Sachiko Mita,[1] Hiroshi Suzuki,[1] Hidetaka Akita,[1] Bruno Stieger,[2] Peter J. Meier,[2] Alan F. Hofmann,[3] and Yuichi Sugiyama[1]

[1]*Graduate School of Pharmaceutical Sciences, The University of Tokyo, 7–3-1 Hongo, Bunkyo-ku, Tokyo, Japan;* [2]*Division of Clinical Pharmacology and Toxicology, Department of Medicine, University Hospital, Zurich, Switzerland; and* [3]*Department of Medicine, University of California, San Diego, California*

Submitted 20 August 2003; accepted in final form 29 July 2004

Mita, Sachiko, Hiroshi Suzuki, Hidetaka Akita, Bruno Stieger, Peter J. Meier,Alan F. Hofmann, and Yuichi Sugiyama. Vectorial transport of bile salts across MDCK cells expressing both rat Na^+-taurocholate cotransporting polypeptide and rat bile salt export pump. *Am J Physiol Gastrointest Liver Physiol* 288: G159–G167, 2005. First published August 5, 2004; doi:10.1152/ajpgi.00360.2003.—Bile salts are predominantly taken up by hepatocytes via the basolateral Na^+-taurocholate cotransporting polypeptide (NTCP/SLC10A1) and secreted into the bile by the bile salt export pump (BSEP/ABCB11). In the present study, we transfected rat Ntcp and rat Bsep into polarized Madin-Darby canine kidney cells and characterized the transport properties of these cells for eight bile salts. Immunohistochemical staining demonstrated that Ntcp was expressed at the basolateral domains, whereas Bsep was expressed at the apical domains. Basal-to-apical transport of taurocholate across the monolayer expressing only Ntcp and that coexpressing Ntcp/Bsep was observed, whereas the flux across the monolayer of control and Bsep-expressing cells was symmetrical. Basal-to-apical transport of taurocholate across Ntcp/Bsep-coexpressing monolayers was significantly higher than that across monolayers expressing only Ntcp. Kinetic analysis of this vectorial transport of taurocholate gave an apparent K_m value of 13.9 ± 4.7 μM for cells expressing Ntcp alone, which is comparable with 22.2 ± 4.5 μM for cells expressing both Ntcp and Bsep and V_{max} values of 15.8 ± 4.2 and 60.8 ± 9.0 pmol·min^{-1}·mg protein^{-1} for Ntcp alone and Ntcp and Bsep-coexpressing cells, respectively. Transcellular transport of cholate, glycocholate, taurochenodeoxycholate, chenodeoxycholate, glycochenodeoxycholate, tauroursodeoxycholate, ursodeoxycholate, and glycoursodeoxycholate, but not that of lithocholate was also observed across the double transfectant. This double-expressing system can be used as a model to clarify vectorial transport of bile salts across hepatocytes under physiological conditions.

bile salt transporters; hepatocyte; transcellular transport

VECTORIAL TRANSPORT OF BILE salts across hepatocytes plays a vital role in their efficient enterohepatic circulation. Indeed, the highly concentrated excretion of bile salts has been demonstrated and the concentration gradient of bile salts is as steep as 100- to 1,000-fold between the portal plasma and bile. This vectorial transport is supported by the transporters located on the basolateral and bile canalicular membranes (18, 33).

On the basolateral membrane of hepatocytes, bile salts are taken up from the portal vein by Na^+-dependent Na^+-taurocholate-(TC) cotransporting polypeptide (Ntcp; rat Ntcp/Slc10a1 and human NTCP/SLC10A1) (10, 11) and Na^+-independent organic anion-transporting polypeptides (rat Oatps/Slc21a and human OATPs/SLC21A). On the bile canalicular membrane, unipolar bile salts are secreted into bile by the apical bile salt export pump (rat Bsep/AbcB11 and human BSEP/ABCB11) (4, 7, 23), whereas dipolar bile salts, which account for only 0.5% of total biliary bile salts in humans, are excreted by multidrug-resistance protein 2 (rat Mrp2/Abcc2 and human MRP2/ABCC2) (13, 14, 32). Thus NTCP/Ntcp and BSEP/Bsep play key roles in the transport of bile salts across hepatocytes.

The molecular properties of these two transporters have been characterized recently. For Ntcp, the transport characteristics were investigated using cRNA-injected oocytes and cDNA-transfected cell lines such as COS-7 (3, 15), Chinese hamster ovary (CHO) (31), HeLa (28), V79, and HPCT-1E3 cells (24). The transport properties of BSEP have been characterized exclusively using cRNA-injected oocytes and isolated membrane vesicles prepared from cDNA-transfected/infected Sf9 cells (1, 4, 7, 9, 23, 30) or mammalian BALB-3T3 fibroblasts (9). Although the uptake and efflux transporters act synergistically to produce the vectorial transport of bile salts, previous analyses have only focused on the function of a single transporter. Therefore, it seemed desirable to establish an in vitro experimental system to allow quantitative analysis of the transcellular transport of bile salts across hepatocytes from blood to bile. Such a synergistic role of transporters may be quantitatively analyzed by examining the transcellular transport of substrates across the cell monolayer after transfection/infection of the respective cDNAs. Indeed, recent studies using a double transfectant of OATP8 and MRP2 (6) and that of OATP2 and MRP2 (26) have demonstrated that this experimental approach is feasible.

In the present study, we have stably transfected rat Ntcp into polarized Madin-Darby canine kidney (MDCK) cells, which were subsequently infected with a recombinant adenovirus containing rat Bsep cDNA. After it was confirmed that Ntcp and Bsep were expressed on the basolateral and apical membranes, respectively, we characterized the transport of a series of bile salts. Kinetic analysis was performed for TC, because this bile salt accounts for >80% of the bile salt pool in rats and is transported by both Ntcp and Bsep (7, 17).

MATERIALS AND METHODS

Chemicals. [^{3}H]cholic acid (24.5 Ci/mmol), [^{3}H]taurocholic acid (2 Ci/mmol), and [^{14}C]chenodeoxycholic acid (48.6 mCi/mmol) were

Address for reprint requests and other correspondence: Y. Sugiyama, Dept. of Molecular Pharmacokinetics, Graduate School of Pharmaceutical Sciences, The Univ. of Tokyo 7-3-1 Hongo, Bunkyo-ku, Tokyo 113–0033, Japan (E-mail: sugiyama@mol.f.u-tokyo.ac.jp).

The costs of publication of this article were defrayed in part by the payment of page charges. The article must therefore be hereby marked "*advertisement*" in accordance with 18 U.S.C. Section 1734 solely to indicate this fact.

purchased from PerkinElmer Life Sciences (Boston, MA). [^{14}C]glycocholic acid (57.3 mCi/mmol) and [^{14}C]lithocholic acid (57.3 mCi/mmol) were purchased from American Radiolabeled Chemicals (St. Louis, MO). [^{3}H]ursodeoxycholic acid (20 Ci/mmol) and unlabeled ursodeoxycholic acid were obtained from SibTech (Newington, CT) by customized synthesis. [^{3}H]taurochenodeoxycholic acid (10 Ci/mmol), [^{3}H]glycochenodeoxycholic acid (11 Ci/mmol), [^{3}H]tauroursodeoxycholic acid (10 Ci/mmol), and [^{3}H]glycoursodeoxycholic acid (11 Ci/mmol) were synthesized in the laboratory of Alan F. Hofmann as described (29). Unlabeled taurocholic acid, taurochenodeoxycholic acid, and glycochenodeoxycholic acid were purchased from Sigma (St. Louis, MO). Unlabeled cholic acid was purchased from Wako Pure Chemicals Industries (Osaka, Japan). Unlabeled ursodeoxycholic acid, tauroursodeoxycholic acid, and glycoursodeoxycholic acid were kindly provided by Mitsubishi Pharma (Osaka, Japan). All other chemicals used were commercially available and of reagent grade.

Antiserum for rat Bsep was raised in rabbits against an oligopeptide (the COOH terminus of rat Bsep; AYYKLVITGAPIS) coupled with keyhole limpet hemocyanin via m-maleimidobenzoyl-*N*-hydroxysuccinimide ester (1). Antiserum for rat Ntcp was raised in rabbits against a COOH-terminal fusion protein of rat Ntcp (31). Antisera against Ntcp and Bsep were used at a dilution of 1:5,000 and 1:1,000 for immunoblotting and 1:250 and 1:50 for immunofluorescence, respectively.

Cell culture and transfection. Parental MDCK cells were cultured in DMEM with 10% fetal bovine serum and 1% antibiotic-antimycotic (GIBCO; 100 U/ml penicillin, 100 μg/ml streptomycin, 0.25 μg/ml amphotericin B) at 37°C under 5% CO_2. Full-length Ntcp cDNA cloned previously in our laboratory (15) was inserted into a mammalian expression vector (pCXN2) (22) and transfected into MDCK cells using LipofectAMINE (Invitrogen Corp., Carlsbad, CA) according to the manufacturer's instructions. Transfectants expressing Ntcp were selected with G418 (600 μg/ml). The clone with the highest Ntcp expression was screened by immunoblot analysis.

Construction of recombinant adenovirus containing rat Bsep. BD Adeno-X Adenoviral Expression System (BD Biosciences, Palo Alto, CA) was used to establish the recombinant adenovirus. Full-length rat Bsep cDNA cloned previously in our laboratory (1) was inserted into pShuttle vector resulting in the production of pShuttle-Bsep, which has an I-CeuI and a PI-SceI site upstream and downstream of the Bsep expression cassette, respectively. The I-CeuI/PI-SceI-digested fragments of pShuttle-Bsep were ligated with I-CeuI/PI-SceI digested Adeno-X Viral DNA (BD Biosciences), resulting in pAd-Bsep. To generate the virus, pAd-Bsep was digested with *Pac*I. Linearized DNA was transfected to HEK-293 cells plated in 12-well dishes with Fugene 6 (Roche Diagnostics, Indianapolis, IN) according to the manufacturer's instructions. Virus (Ad-Bsep) was prepared as described previously (19). Viruses were purified by CsCl gradient centrifugation, dialyzed against a solution containing 10 mM Tris (pH 7.5), 1 mM $MgCl_2$, and 10% glycerol and stored in aliquots at −80°C. Viral titers were determined as described previously (20).

Immunoblot analysis. MDCK cells transfected with Ntcp or vector were infected by the recombinant adenoviruses containing the cDNAs for Bsep or green fluorescent protein (GFP) at a multiplicity of infection (MOI) of 250. Cells were harvested 24 h after infection, and the expression of Ntcp was induced with 5 mM sodium butyrate. After 24 h, crude membrane fractions were prepared from cultured MDCK cells as described earlier (12). Specimens were dissolved in 3× SDS sample buffer (New England Biolabs, Beverly, MA) and transferred to a 12.5 or 8.5% SDS-PAGE plate with a 3.75% stacking gel. The molecular weight was determined using a prestained protein marker (New England Biolabs). Proteins were transferred onto a polyvinylidene difluoride membrane (Pall, NY) using a blotter (Trans-blot; Bio-Rad, Richmond, CA) at 15 V for 1 h. The membrane was blocked with Tris-buffered saline containing 0.05% Tween 20 (TBS-T) and 5% skimmed milk for 1 h at room temperature. After being washed with TBS-T, the membrane was incubated with anti-Ntcp serum (dilution 1:1,000) or anti-Bsep serum (dilution 1:1,000). The membrane was allowed to bind a horseradish peroxidase-labeled anti-rabbit IgG antibody (Amersham Biosciences, Piscataway, NJ) diluted 1:2,000 in TBS-T for 1 h at room temperature followed by washing with TBS-T.

Confocal laser-scanning immunofluorescence microscopy. Ntcp- or vector-transfected confluent MDCK cells were grown on coverslips for 2 days and infected by recombinant adenovirus containing the cDNA for Bsep or GFP (250 MOI). Cells were harvested 24 h after infection, and expression of Ntcp was induced with 10 mM sodium butyrate. Twenty-four hours after induction, cells were fixed with ice-cold methanol for 10 min, permeabilized with 1% Triton X-100 in PBS for 10 min, and incubated for 1 h with primary antibodies at room temperature. After this, cells were washed three times with PBS and incubated with goat anti-rabbit IgG Alexa Flour 488 (Molecular Probes, Eugene, OR), diluted 250-fold in PBS for 1 h at room temperature, and mounted in VECTASHIELD mounting medium (Vector Laboratories, Burlingame, CA). Confocal laser-scanning microscopy was performed with an LSM 510 microscope from Zeiss (Oberkochen, Germany).

Transport assays. Ntcp- or vector-transfected MDCK cells were seeded on transwell membrane inserts (pore size of 3 μm; Falcon, Bedford, MA) in 24-well plates at a density of 1.4×10^5 cells per insert and cultured at confluence for 2 days and infected by recombinant adenovirus containing cDNAs for Bsep or GFP (250 MOI). Cells were harvested 48 h after infection, and expression of Ntcp was induced with 10 mM sodium butyrate (5). Then, 24 h after induction, cells were washed with transport buffer (in mM: 118 NaCl, 23.8 $NaHCO_3$, 4.83 KCl, 0.96 KH_2PO_4, 1.20 $MgSO_4$, 12.5 HEPES, 5 glucose, and 1.53 $CaCl_2$ adjusted to pH 7.4). Subsequently, ^{3}H- or ^{14}C-labeled substrates were added to the transport buffer in either the apical (250 μl) or basal compartment (950 μl). After the times indicated, the radioactivity in the opposite compartment was measured. The intracellular accumulation of radioactivity was determined at the end of the experiments by lysing the cells with 500 μl 0.2 N NaOH in distilled water and measuring the radioactivity in the cell lysates. Aliquots (50 μl) of cell lysate were used to determine protein concentrations by the method of Lowry et al. (16) with bovine serum albumin as a standard. The apparent intracellular concentration of substrates was determined by assuming that the cellular volume per milligram cellular protein was 4 μl.

Data analysis. For the kinetic analysis, the transcellular transport of TC determined over 2 h was used. The transcellular transport at 30 and 60 min was also determined to confirm that the transcellular transport determined over 2 h represents the initial rate of flux (data not shown). The apparent kinetic parameters for transcellular transport of TC were estimated according to the Michaelis-Menten equation by assuming one saturable and one nonsaturable component: $v_0 = (V_{max} \times S)/(K_m + S) + PS_{diff} \times S$, where v_0 is the initial transport velocity of substrates (pmol·min^{-1}·mg protein^{-1}), S is the substrate concentration in medium (μM), K_m is the Michaelis constant (μM), V_{max} is the maximum uptake rate (pmol·min^{-1}·mg protein^{-1}), and PS_{diff} is the nonsaturable permeability surface area (PS) product expressed as clearance (μl·min^{-1}·mg protein^{-1}). The uptake data were fitted to this equation by a nonlinear least-squares method with a MULTI program (34) to obtain estimates of the kinetic parameters. The input data were weighted as the reciprocals of the squares of the observed values.

Kinetic analysis of the transcellular transport was performed according to the following procedure. The rate of appearance of ligands in the apical compartment is described by

$$dx_{apical}/dt = PS_{net} \times C_{med} \quad (1)$$

where x_{apical} (pmol/mg protein) is the amount of ligand in the apical compartment, and PS_{net} (μl·min^{-1}·mg protein^{-1}) is the PS product defined for the ligand concentration in the medium [C_{med} (pmol/μl)].

The rate of accumulation of ligands in the apical compartment is also described by

$$dx_{apical}/dt = PS_{apical} \times C_{cell} \quad (2)$$

where PS_{apical} ($\mu l \cdot min^{-1} \cdot mg\ protein^{-1}$) is the clearance for the efflux of ligand across the apical membrane, which is defined for the ligand concentration in the cells [C_{cell} (pmol/μl)]. In addition, the mass-balance of ligand in the cells can be described by

$$dx_{cell}/dt = PS_{basal} \times C_{med} - (PS_{apical} + PS_{basal,eff}) \times C_{cell} \quad (3)$$

where x_{cell} (pmol/mg protein) is the amount of ligand in the cells, PS_{basal} ($\mu l \cdot min^{-1} \cdot mg\ protein^{-1}$) is the clearance for the influx of ligand across the basal membrane, which is defined for C_{med}, and $PS_{basal,eff}$ ($\mu l \cdot min^{-1} \cdot mg\ protein^{-1}$) is the clearance for the efflux of ligand across the basal membrane from the cell to the basal compartment, which is defined for C_{cell}, respectively.

At steady-state ($dx_{cell}/dt = 0$) , *Eq. 3* is simplified to *Eq. 4*, which gives the cell-to-medium concentration ratio at steady state ($C_{cell,ss}/C_{med,ss}$)

$$C_{cell,ss}/C_{med,ss} = PS_{basal}/(PS_{apical} + PS_{basal,eff}) \quad (4)$$

From Eqs. *1*, *2*, and *4*, PS_{net} is given as a hybrid parameter consisting of PS_{basal}, PS_{apical}, and $PS_{basal,eff}$

$$PS_{net} = PS_{basal} \cdot PS_{apical}/(PS_{apical} + PS_{basal,eff}) \quad (5)$$

Under conditions where $PS_{apical} \gg PS_{basal,eff}$, PS_{net} can be approximated

$$PS_{net} \approx PS_{basal} \quad (6)$$

In the present study, PS_{net} and PS_{apical} were calculated by dividing the rate for the transcellular transport of ligands determined over 2 h by the medium concentration of ligands and by the apparent cellular concentration of ligands determined at the end of the experiments (2 h), respectively. When $PS_{apical} \gg PS_{basal,eff}$ for Ntcp and Bsep coexpressing MDCK (MDCK-Ntcp/Bsep) and Bsep expressing MDCK monolayers (MDCK-Bsep), the difference between PS_{net} for $_{MDCK\text{-}Ntcp/Bsep}$ and PS_{net} for MDCK-Bsep represents the clearance for the uptake mediated by Ntcp (PS_{Ntcp}). Consequently, PS_{Ntcp} was calculated according to

$$PS_{Ntcp} = PS_{net\ for\ MDCK\text{-}Ntcp/Bsep} - PS_{net\ for\ MDCK\text{-}Bsep} \quad (7)$$

RESULTS

Expression and localization of Ntcp and Bsep in MDCK cells. The expression of Ntcp and Bsep in the transfected MDCK cells was analyzed by immunoblotting (Fig. 1). As shown in Fig. 1*A*, Ntcp expression was detectable as a band of 55 kDa in MDCK-Ntcp and MDCK-Ntcp/Bsep. The expression of Bsep was also detectable at 160 kDa in MDCK cells transfected with Bsep cDNA (MDCK-Bsep) and in MDCK-Ntcp/Bsep cells (Fig. 1*B*). In the control MDCK cells, no expression of Ntcp or Bsep could be detected (Fig. 1).

The cellular localization of the recombinant transporters in the transfectants was assessed using confocal laser-scanning microscopy. In MDCK-Ntcp and MDCK-Ntcp/Bsep cells, Ntcp was localized on the basolateral membrane (Fig. 2, *A* and *C-1*). In MDCK-Bsep and MDCK-Ntcp/Bsep cells, Bsep was localized on the apical membrane (Fig. 2, *B* and *C-2*).

In the present study, we infected the MDCK cells stably expressing Ntcp with recombinant adenoviruses containing Bsep cDNA. Because the Ntcp expressing MDCK cells were prepared by incubating the cells in the presence of G418 after transfection of plasmid vector containing Ntcp cDNA and neomycin resistance gene, all the cells used in the present study express Ntcp as shown in Fig. 2. In contrast, immunohistochemical studies indicated that the expression of Bsep was detectable in 5–10% of the infected cells (Fig. 2). However, the expression rate of Bsep may be higher because it is possible that there were Bsep-expressing cells at a low level that was under the detection limit of the immunohistochemical staining. Although we infected the cells with the recombinant adenoviruses at more than 250 MOI, infection of the viruses at this higher MOI resulted in the death of the cells presumably due to the toxicity of the viruses.

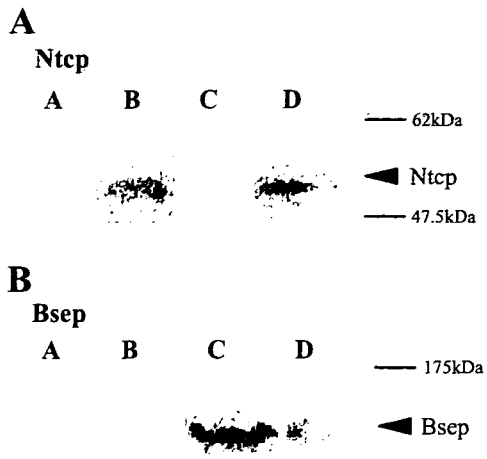

Fig. 1. Western blot analysis of Na^+-taurocholate-(TC) cotransporting polypeptide (Ntcp) and bile salt export pump (Bsep). The expression level of Ntcp and Bsep was determined by Western blot analysis. Crude membrane fractions (30 μg) from the control, Madin-Darby canine kidney (MDCK)-Ntcp, MDCK-Bsep, and MDCK-Ntcp/Bsep cells were separated on 12.5 and 8.5% SDS-PAGE for Ntcp (*A*) and Bsep (*B*), respectively.

Transcellular transport of [^{3}H]TC mediated by Ntcp and Bsep. The function of Ntcp and Bsep was studied by measuring the transcellular transport of TC across the monolayers. In the case of the control cells (Fig. 3*A*) and cells expressing only Bsep (Fig. 3*C*), there was little transport of TC. Vectorial transport in the apical direction was present in MDCK-Ntcp (Fig. 3*B*) and MDCK-Ntcp/Bsep monolayers (Fig. 3*D*). The basal-to-apical flux of TC across the MDCK-Ntcp/Bsep monolayer was significantly higher than that across the MDCK-Ntcp monolayer (Fig. 3). In addition, [^{3}H]TC remaining in the cells at the end of the experiment (2 h) of the doubly transfected cells (56.3 ± 1.2 pmol/mg protein, means ± SE, n = 3) was significantly lower than that present in the Ntcp-transfected cells (130 ± 9 pmol/mg protein). The marked increase in vectorial transport when Ntcp alone was expressed (Fig. 3*B*) indicates the presence of apical non-Bsep transporters for TC.

The basal-to-apical flux of TC across MDCK-Ntcp and MDCK-Ntcp/Bsep monolayers was saturable (Fig. 4). The kinetic studies were performed by analyzing the transcellular transport for 2 h. Because the amount of bile salts transported increased linearly as a function of time over the period of 2 h (Fig. 3), the initial transport velocity can be determined from the slope. Kinetic analysis revealed that the saturation was best described by assuming the presence of one saturable and one nonsaturable component (Fig. 4*A*). Figure 4*B* represents the saturation of the transporter-mediated transport of TC, which was obtained by subtracting the transport across the control cells ($PS_{diff} \times S$) from the transport across MDCK-Ntcp and

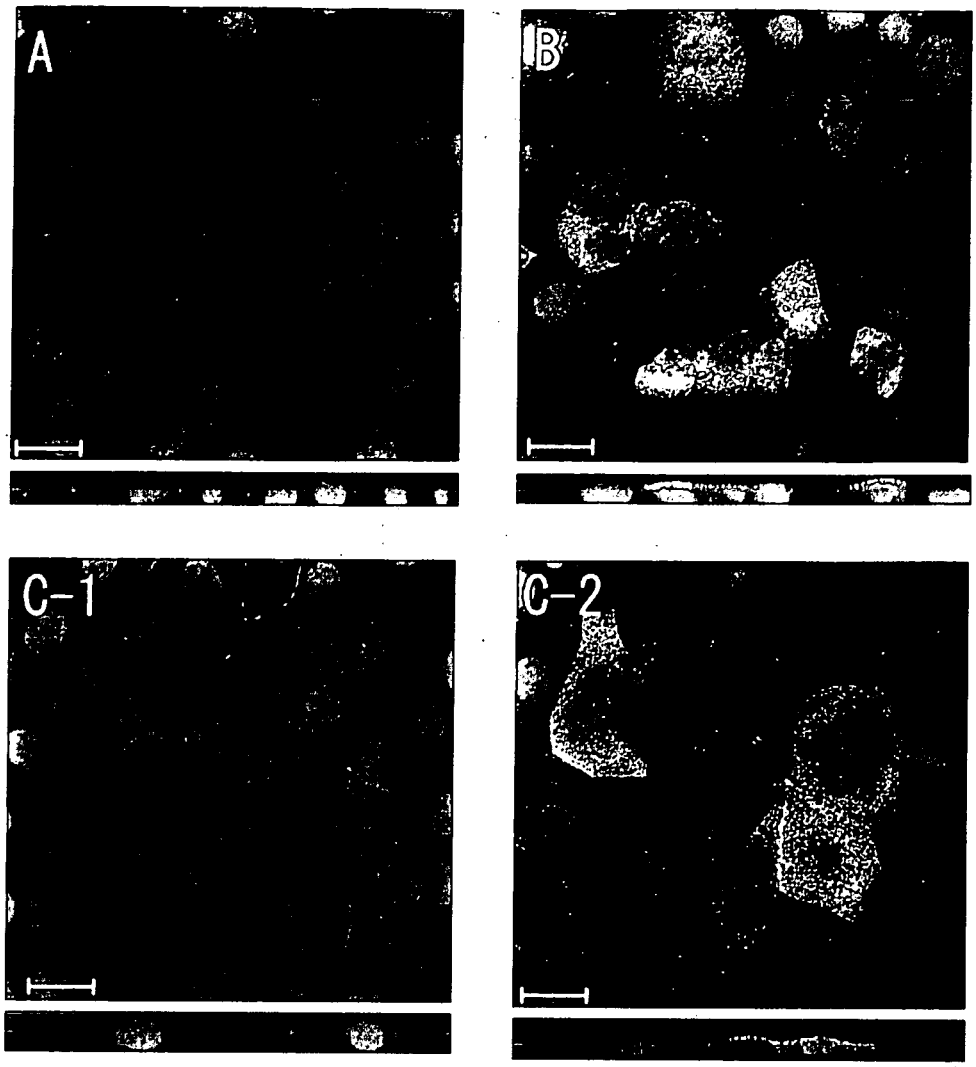

Fig. 2. Immunolocalization of Ntcp and Bsep in MDCK cells. The localization of Ntcp and Bsep was confirmed in MDCK cells. MDCK-Ntcp (*A*), MDCK-Bsep (*B*), and MDCK-Ntcp/Bsep (*C*) cells were stained with rabbit antiserum against Ntcp (*A* and *C-1*; red fluorescence) or Bsep (*B* and *C-2*; green fluorescence). Nuclei were stained with TOPRO-3 (blue fluorescence). In *A–C-2*, *top* shows the en face image and *bottom* shows the Z-sectioning image with a horizontal line in the en face image. Bar, 20 μm.

MDCK-Ntcp/Bsep cells. The analysis gave K_m values of 22.2 ± 4.5 μM for doubly transfected cells and 13.9 ± 4.7 μM for Ntcp transfected cells. The V_{max} values were 60.8 ± 9.0 and 15.8 ± 4.2 pmol·min^{-1}·mg protein^{-1} for doubly transfected and Ntcp-transfected cells, respectively. The PS_{diff} was unaffected by Bsep transfection. The PS_{diff} values were 0.10 ± 0.04 μl·min^{-1}·mg protein^{-1} for doubly transfected cells and 0.12 ± 0.03 μl·min^{-1}·mg protein^{-1} for Ntcp transfected cells.

Further evidence that the transfection of Bsep had a powerful influence was shown by the saturation of the PS_{apical} (Fig. 5). As the medium TC concentration was increased to 300 μM, the PS_{apical} in the MDCK-Ntcp/Bsep monolayer became saturated to the same level as the control and MDCK-Ntcp monolayers (Fig. 5). PS_{apical} was almost the same for the control and MDCK-Ntcp monolayers, and no saturation was observed in these monolayers.

Transcellular transport of a series of bile salts across MDCK monolayers. In addition to TC, the transcellular transport of a variety of natural conjugated and unconjugated bile salts was characterized. For conjugated bile salts, fluxes across the parental MDCK monolayer were symmetrical and extremely low (Fig. 6). Insertion of Ntcp (Fig. 6*B*) caused a marked increase in vectorial transport of taurochenodeoxycholate (TCDC), glycochenodeoxycholate (GCDC), tauroursodeoxycholate (TUDC), glycoursodeoxycholate (GUDC), and TC (shown previously in Fig. 3), indicating the presence of non-Bsep apical transporters (Fig. 6). Glycocholate (GC) transport increased to a much lower degree. Insertion of both transporters caused a marked increase in vectorial transport of all conjugated bile salts except TCDC and TUDC, the vectorial transport of which in the absence of Bsep was already far higher than that of any other bile salt (Fig. 6).

For unconjugated bile salts (Fig. 7), there was symmetrical transport in the parental MDCK monolayers. The magnitude of transport varied in direct proportion to the passive membrane permeability (hydrophobicity) of individual bile salts [lithocholate (LCA) > chenodeoxycholate (CDCA) = ursodeoxycholate (UDCA) > cholate (CA); Fig. 7]. Addition of Ntcp increased the transport of CDCA but not that of other unconjugated bile salt (Fig. 7). In the doubly transfected cells, vectorial transport of CA, CDCA, and UDCA but not that of LCA was observed (Fig. 7).

Finally, the PS_{Ntcp} of these bile salts was calculated to quantitatively evaluate the role of basolateral transport in their transcellular transport. Figure 8 shows the PS_{Ntcp} of these bile salts normalized with respect to that of TC. The rank order for

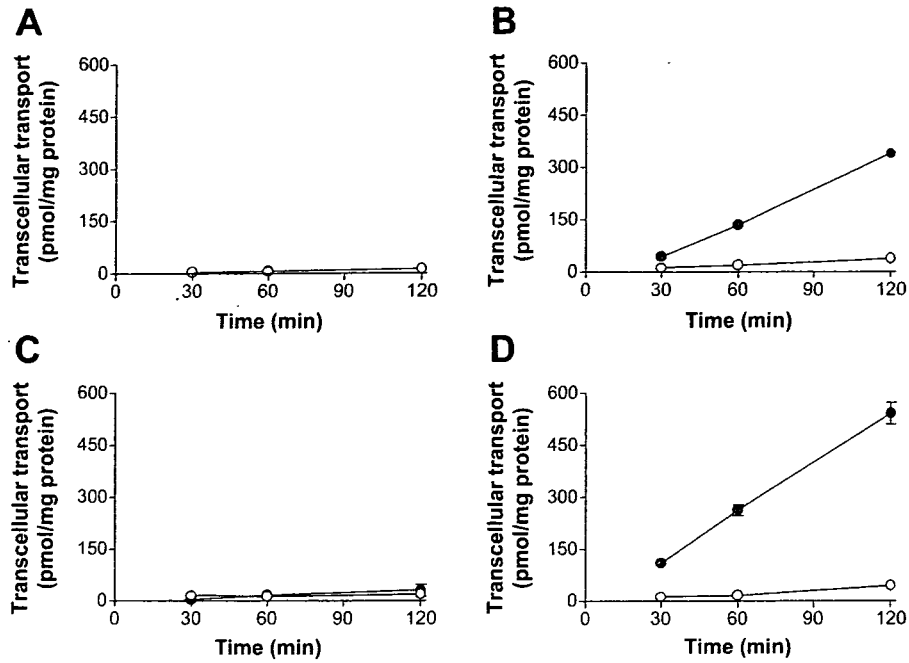

Fig. 3. Time profiles of the transcellular transport of [^{3}H]TC across MDCK monolayers. Transcellular transport of [^{3}H]TC (1 μM) across MDCK monolayers was examined as a function of time. *A-D* represent the data for the control, MDCK-Ntcp, MDCK-Bsep, and MDCK-Ntcp/Bsep monolayers, respectively. ○ And ● represent the transcellular transport in the apical-to-basal and basal-to-apical directions, respectively. Each point and vertical bar represents the mean ± SE of 3 determinations. Where vertical bars are not shown, the SE was contained within the limits of the symbol.

PS_{Ntcp} was TUDC > TCDC > GCDC > GUDC, TC, CDCA > UDCA > GC > CA.

DISCUSSION

Hepatic vectorial transport of bile salts is supported by the uptake and efflux transporters located on the sinusoidal and bile canalicular membrane, respectively. Although the molecular properties of these two transporters have been separately characterized, there has been no description of the functional coexpression system of these transporters. In the present study, we have established MDCK cells expressing both rat bile salt uptake transporter (Ntcp) and rat bile salt efflux transporter (Bsep).

Basolateral and apical localization of Ntcp and Bsep, respectively, was confirmed by immunohistochemical analysis (Fig. 2), which is consistent with the localization in rat hepatocytes (7, 31). Although the transport of TC across the control and MDCK-Bsep was symmetrical, this bile salt was transported from the basal side to the apical side across MDCK-Ntcp and MDCK-Ntcp/Bsep monolayers (Fig. 3, *B* and *D*). Furthermore, the transcellular transport across MDCK-Ntcp/Bsep monolayers was significantly higher than that across MDCK-Ntcp monolayers (Fig. 3, *B* and *D*). These results indicate that Ntcp and Bsep exhibit a coupled transport function in this expression system. TC molecules in the basal compartment are taken up by Ntcp into the cells and then exported to the apical compartment by Bsep. The function of Bsep was further confirmed by the fact that the cellular accumulation of TC, which was determined at the end of the experiments, was significantly lower in MDCK-Ntcp/Bsep cells compared with MDCK-Ntcp cells (see RESULTS). The significant basal-to-apical flux of TC across MDCK-Ntcp indicates the presence of endogenous transporter(s) on the apical membrane, capable of extruding this bile salt from the cells (Fig. 3*B*). At the present moment, we cannot identify this endogenous transporter. Although it has been suggested that MDR1, MRPs, and OATPs are expressed endogenously in MDCK cells (8, 21), they cannot be candidates, if we consider their cellular localization and substrate specificity. However, we were able to analyze the transport mediated by Bsep, because basal-to-apical flux was significantly enhanced by the additional expression of Bsep (MDCK-Ntcp/Bsep monolayer), compared with the flux mediated by

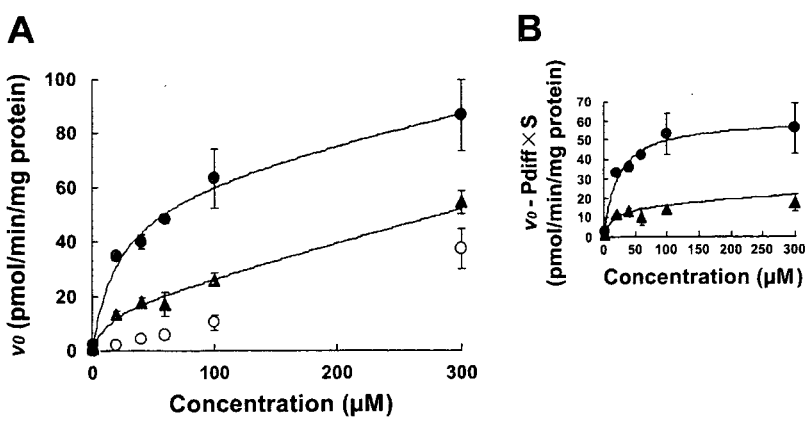

Fig. 4. Concentration dependence of the transcellular transport of [^{3}H]TC across Ntcp- and Bsep-expressing MDCK monolayers. The saturation of the basal-to-apical flux of [^{3}H]TC (1 μM) across MDCK-Ntcp (▲), MDCK-Ntcp/Bsep (double transfectant; ●), and control MDCK monolayers (○) was studied for 2 h in the presence and absence of unlabeled TC at 37°C (*A*). Each symbol and bar represent the mean ± SE of 3 determinations. The solid lines represent the fitted line. *B* represents the saturation of transporter-mediated transport of TC, which was obtained by subtracting the transport across the control cells [nonsaturable permeability surface (PS) area ($PS_{diff} \times S$)] from the transport across MDCK-Ntcp and MDCK-Ntcp/Bsep cells (▲ and ●, respectively). v_0, Initial transport velocity of substrates.

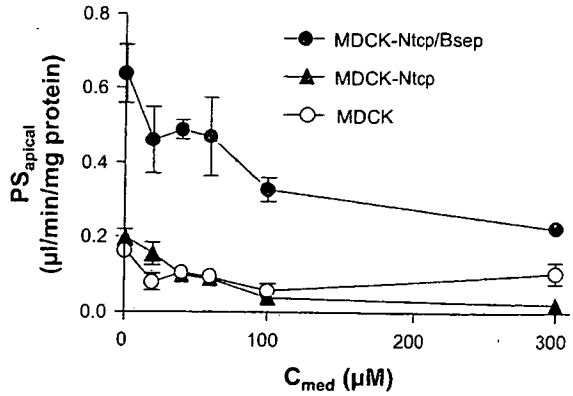

Fig. 5. Concentration dependence of the transport of [^{3}H]TC across the apical membrane of MDCK cells. The clearance of the transport of TC across the apical membrane of MDCK monolayers (PS_{apical}) was determined by dividing the amount of transcellularly transported TC by the apparent intracellular concentration of TC (C_{cell}; μM). The PS_{apical} values of MDCK-Ntcp/Bsep (double transfectant; ●), MDCK-Ntcp (▲), and control MDCK monolayers (○) were plotted against the medium concentration of TC (C_{med}; μM). Each symbol and bar represent the means ± SE of 3 determinations.

Ntcp and endogenous transporters in the MDCK monolayer (MDCK-Ntcp monolayer; Fig. 3, *B* and *D*).

The saturation of transport was examined using MDCK-Ntcp and MDCK-Ntcp/Bsep monolayers, which exhibit significant basal-to-apical transport of TC. The basal-to-apical flux of TC across MDCK-Ntcp and MDCK-Ntcp/Bsep monolayers was saturated with apparent K_m values of 13.9 ± 4.7 and 22.2 ± 4.5 μM, respectively (Fig. 4). These K_m values are similar to the reported K_m value of TC for Ntcp [34 μM; (27)], which indicates that the basal-to-apical flux of TC across MDCK-Ntcp/Bsep is dominated by the influx clearance of Ntcp. This in vitro result is consistent with our previous studies performed in situ. Previously, we performed liver perfusion studies and found that the canalicular efflux clearance (PS_{apical}) of TC is much larger than the basolateral efflux clearance ($PS_{basal,eff}$): 69.2 ± 6.3 vs. 8.4 ± 0.6 $\mu l \cdot min^{-1} \cdot g\ liver^{-1}$ (2). From this result, we can conclude that the basal-to-apical flux of TC across hepatocytes is dominated by influx clearance under physiological conditions (see *Eq. 6*). However, to compare in vitro and in vivo results, the expression level of Ntcp and Bsep should be compared. Moreover, we have to consider the presence of other bile salt transport systems in the hepatocytes, such as uptake transporters (Oatps) and Mrp4, an efflux transporter, located on the basolateral membrane of hepatocytes (25).

The saturation of PS_{apical} was also examined. At lower and presumably physiological medium concentrations of TC (less than ~20 μM), PS_{apical} in the MDCK-Ntcp/Bsep monolayer was significantly higher than that in the MDCK-Ntcp monolayer, the latter being comparable with that in the control MDCK monolayer (Fig. 5). As the medium TC concentration was increased to 300 μM, the PS_{apical} in the MDCK-Ntcp/Bsep monolayer became saturated to the same level as the control and MDCK-Ntcp monolayers (Fig. 5). Although the K_m value of Bsep-mediated TC transport is reported to be 5.3 μM (7), we cannot determine this K_m value from the results of the present experiment because of the fact that it is difficult to determine the intracellular unbound concentration of TC in MDCK-Ntcp/Bsep cells.

Transcellular transport of other kinds of bile salts was also examined. GC, TCDC, GCDC, TUDC, GUDC (Fig. 6*D*), CA, CDCA, and UDCA (Fig. 7*D*) were transported by the MDCK-Ntcp/Bsep monolayer in a vectorial manner. The transcellular transport across the MDCK-Ntcp/Bsep monolayer (Figs. 6*D* and 7*D*) was significantly higher than the control (Figs. 6*A* and 7*A*), MDCK-Ntcp (Figs. 6*B* and 7*B*), and MDCK-Bsep (Figs. 6*C* and 7*C*) monolayers except for TCDC and TUDC. This result suggests that these bile salts, except for TCDC and TUDC, are substrates of Ntcp and Bsep. Among these bile salts, TCDC, TUDC, TC, CA, and GC have been reported to be transported by Ntcp expressing oocytes and CHO9–6 cells (17, 27) and TCDC, GCDC, TUDC, TC, and GC have been reported to be transported by rat Bsep expressing Sf9 vesicles (7, 30). In the present study, we also detected the Ntcp-mediated transport of CDCA, UDCA, GCDC, and GUDC and the Bsep-mediated transport of UDCA, GUDC, CDCA, and CA. Identification of some new substrates of Ntcp and Bsep shows that this model is available for the characterization of these transporters. The transcellular transport of TCDC and TUDC across MDCK-Ntcp (Fig. 6*B*) was not enhanced by the additional expression of Bsep [MDCK-Ntcp/Bsep (Fig. 6*D*)], although this bile salt is reported to be transported by Bsep (7, 30). This difference may be accounted for by assuming that the transport capacity of endogenous (non-Bsep) transporter(s) in MDCK cells is high enough for TCDC and TUDC and, therefore, the rate-determining process for the transcellular transport of these bile salts is the uptake mediated by Ntcp. For LCA, no vectorial transport across the MDCK-Ntcp/Bsep was detectable (Fig. 7), which suggests that this bile salt is a poor substrate of Ntcp and/or Bsep.

Furthermore, to quantitatively evaluate the transcellular transport of these bile salts, the calculated PS_{Ntcp} values were compared (Fig. 8). PS_{Ntcp} was calculated using *Eq. 7*, which is applicable under steady-state conditions ($dx_{cell}/dt = 0$). Although the PS_{Ntcp} values were determined from the results of transcellular transport experiments for 2 h, the fact that the x_{cell} of TC at 2 h (130 ± 9 pmol/mg protein) is the same as that at 10 min (133 ± 30 pmol/mg protein) suggests that the $dx_{cell}/dt = 0$ holds true for up to 2 h. On the basis of this consideration, the analysis method was validated. The rank order for PS_{Ntcp} was TUDC > TCDC > GCDC > GUDC, TC, CDCA > UDCA > GC > CA. This order is the same as that reported previously using recombinant Ntcp; Meier et al. (17) have reported the following rank order: TUDC > TCDC > TC > GC > CA. These data are consistent with the hypothesis that the rate-determining process for the transcellular transport across MDCK-Ntcp/Bsep cells is the uptake process mediated by Ntcp, due to the efficient efflux mediated by Bsep. The fact that taurine-conjugated bile salts are transported to a greater extent than their corresponding glycine or unconjugated derivatives (TC > GC > CA, TCDC > GCDC > CDCA and TUDC > GUDC > UDCA) may be reasonable considering the bile salt composition of rats in which most of the bile salts are taurine conjugates. We were thus able to establish an in vitro model to quantitatively evaluate the vectorial transport of bile salts. However, in the calculation of PS_{Ntcp}, it is assumed that the rate-determining process for the transcellular transport of a series of bile salts is the uptake mediated by Ntcp, as suggested for TC. If this assumption does not hold true for other bile salts,

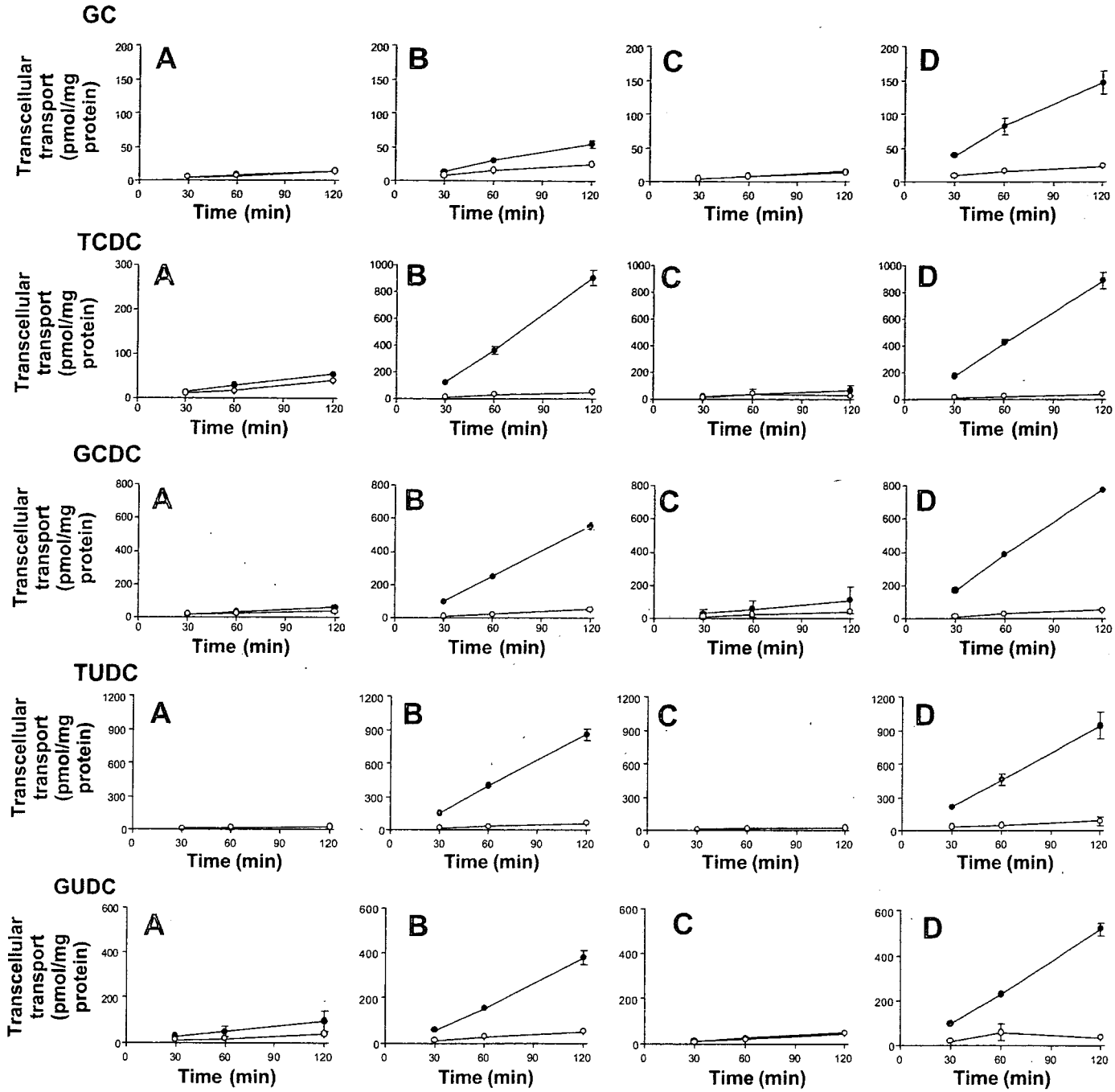

Fig. 6. Time profiles for the transcellular transport of conjugated bile salts across MDCK monolayers. Transcellular transport of [^{14}C]glycocholate (GC), [^{3}H]taurochenodeoxycholate (TCDC), [^{3}H]glycochenodeoxycholate (GCDC), [^{3}H]tauroursodeoxycholate (TUDC), and [^{3}H]glycoursodeoxycholate (GUDC; 1 μM) across the control (*A*), MDCK-Ntcp (*B*), MDCK-Bsep (*C*), and MDCK-Ntcp/Bsep monolayers (*D*) was determined as a function of time. ○ And ● represent the transcellular transport in the apical-to-basal and basal-to-apical directions, respectively. Each point and vertical bar represents the mean ± SE of 3 determinations. Where vertical bars are not shown, the SE was contained within the limits of the symbol.

the calculated PS_{Ntcp} values cannot be compared among bile salts.

This expression system may also be useful for the detecting the transport of bile salts mediated by Bsep. Until now, it has been difficult to study Bsep function in intact mammalian cells because most Bsep substrates are negatively charged under physiological conditions and thus cannot penetrate the cell membrane without the aid of uptake transporters. Therefore, Bsep has been studied using inside-out membrane vesicles prepared from Bsep-expressing cells. With the aid of MDCK-Ntcp/Bsep monolayers, Bsep function can be studied more effectively and sensitively compared with the current in vitro methods using isolated membrane vesicles. Indeed, using MDCK/Ntcp-Bsep monolayers, we could detect the Bsep-mediated transport of CA (Fig. 7), which has not been detectable previously using isolated membrane vesicles. Because the

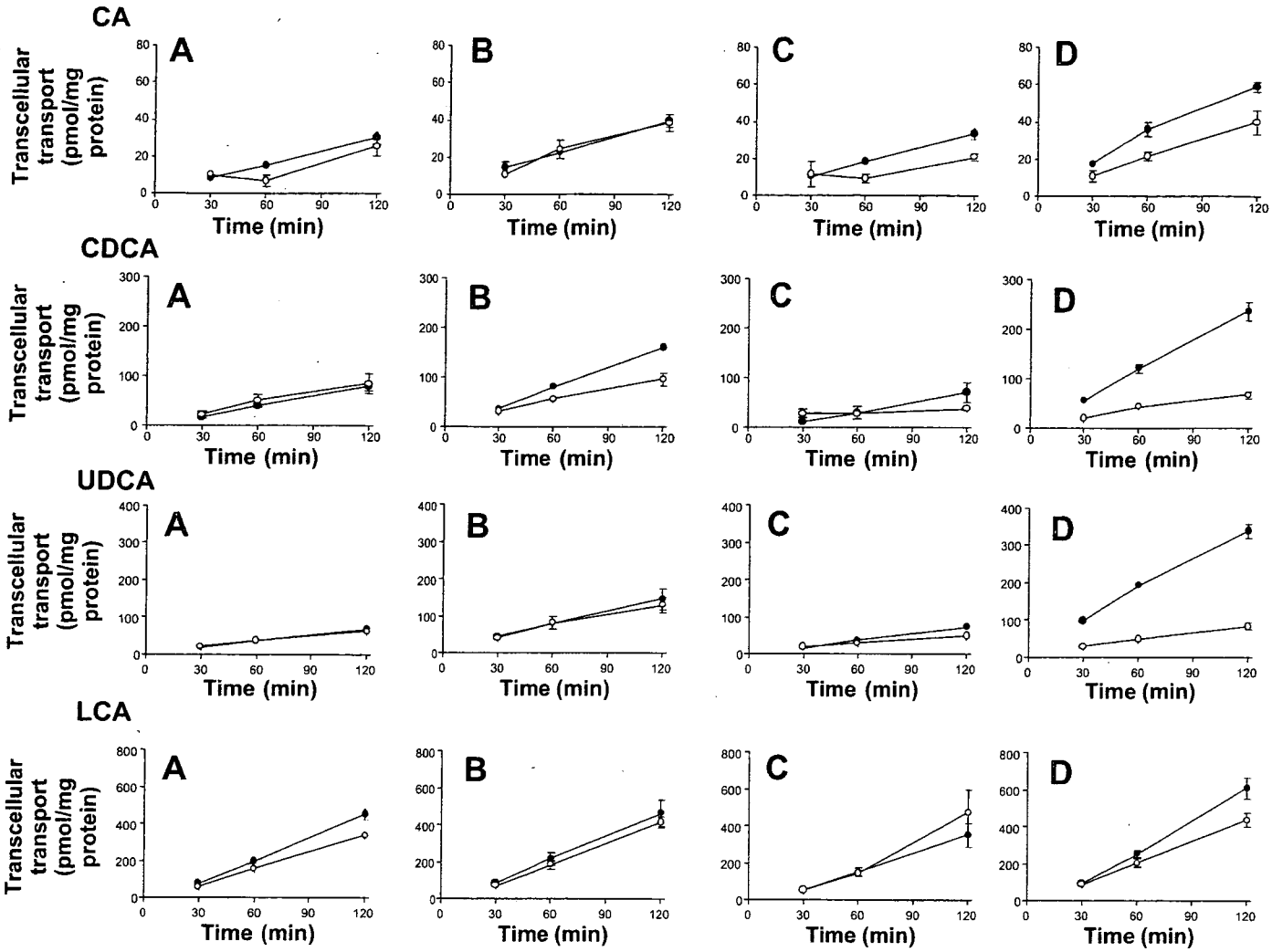

Fig. 7. Time profiles for the transcellular transport of unconjugated bile salts across MDCK monolayers. Transcellular transport of [^{3}H]cholate (CA), [^{14}C]chenodeoxycholate (CDCA), [^{14}C]lithocholate (LCA), and [^{3}H]ursodeoxycholate (UDCA; 1 μM) across the control (*A*), MDCK-Ntcp (*B*), MDCK-Bsep (*C*), and MDCK-Ntcp/Bsep monolayers (*D*) was determined as a function of time. ○ And ● represent the transcellular transport in the apical-to-basal and basal-to-apical directions, respectively. Each point and vertical bar represent the mean ± SE of 3 determinations. Where vertical bars are not shown, the SE was contained within the limits of the symbol.

transported compound is accumulated in the aqueous fluid of the apical compartment, it is easy to detect the transport mediated by Ntcp and/or Bsep due to the low background level; if the uptake of ligands into the cells and/or isolated membrane vesicles is examined, the extent of adsorption to the surface of the cells/membrane vesicles is not negligible. Detection of unlabeled bile salts from the aqueous specimens may be possible with the aid of LC-MS.

In conclusion, we have established MDCK cells expressing both basolateral Ntcp and apical Bsep that transport conjugated and unconjugated bile salts vectorially. Kinetic analysis of the transcellular transport of bile salts suggests that the Ntcp/Bsep coexpressing MDCK monolayer may be useful in analyzing the vectorial transport of individual bile salts. Our system may also be useful for analyzing the inhibitory effects of some compounds on Ntcp and/or Bsep function. Such analysis will give us suggestions for understanding of human cholestatic liver disease induced by the inhibition of NTCP and/or BSEP by drugs.

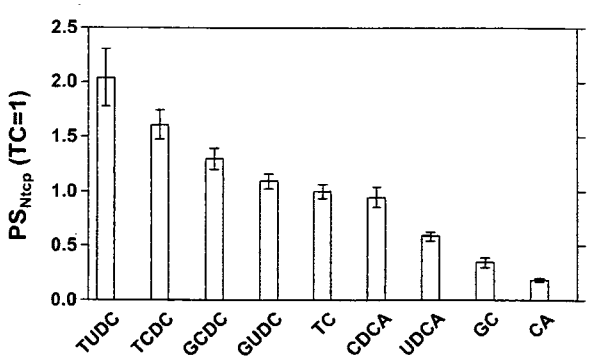

Fig. 8. Comparison of the transcellular transport of bile salts across MDCK monolayer expressing both Ntcp and Bsep. On the basis of the results shown in Fig. 6, the PS_{ntcp} was calculated for CA, GC, TCDC, GCDC, CDCA, TUDC, GUDC, and UDCA (1 μM) according to *Eq. 7* in the text. The PS_{Ntcp} of each bile salt was divided by that of TC. Data represent means ± SE.